August 2021

Fluid Rheological Effects on Insulator-Based Dielectrophoresis

Joseph Armakan Bentor
Clemson University, jbentor@clemson.edu

FLUID RHEOLOGICAL EFFECTS ON INSULATOR-BASED DIELECTROPHORESIS

A Thesis
Presented to
the Graduate School of
Clemson University

In Partial Fulfillment
of the Requirements for the Degree
Master of Science
Mechanical Engineering

---

by
Joseph A. Bentor
August 2021

Accepted by:
Dr. Xiangchun Xuan, Committee Chair
Dr. Rodrigo Martinez-Duarte
Dr. Phanindra Tallapragada

ABSTRACT

Insulator-based dielectrophoresis (iDEP) has been increasingly used to focus, trap and separate particles and cells for various microfluidic applications in the fields of analytical chemistry, bioanalysis, cell biology and clinics etc. It exploits insulating structure(s) to create electric field gradients for dielectrophoretic manipulation of particles and cells in microchannels. However, iDEP has thus far been demonstrated to work with Newtonian fluids only in the majority of the reported applications. As many of the biological (e.g., blood, saliva, DNA solutions, etc.) and chemical (e.g., polymer and colloidal solutions) fluids exhibit non-Newtonian behaviors, it is important and necessary to understand how the fluid rheological properties may affect iDEP. This thesis is aimed to investigate experimentally the effects of fluid elasticity and shear thinning on the iDEP focusing and trapping of particles as well as the electroosmotic flow pattern in two types of microchannels.

In the first experiment we study the fluid rheological effects on iDEP focusing and trapping of polystyrene particles in polyethylene oxide (PEO), xanthan gum (XG) and polyacrylamide (PAA) solutions through a constricted microchannel. Such a geometry is the simplest while the most often used structure in iDEP microdevices. Particle focusing and trapping in the mildly viscoelastic PEO solution are found to be slightly weaker than in the Newtonian buffer. They are, however, significantly improved in the strongly viscoelastic and shear thinning PAA solution. These observed particle focusing behaviors exhibit a similar trend with respect to electric field, which is consistent with a revised theoretical analysis for iDEP focusing in non-Newtonian fluids. No apparent focusing of particles is achieved in the XG solution though the iDEP trapping can take place under a much larger electric field than the other fluids. This is

attributed to the strong shear thinning-induced influences on both the electroosmotic flow and electrokinetic/dielectrophoretic motions.

In the second experiment we investigate the iDEP focusing and trapping of polystyrene particles in the same three types of polymer solutions in a post-array microchannel. Such a geometry has been frequently used to manipulate small particles with submicron and even nanometer sizes. The array of posts causes continuous changes in the non-Newtonian fluid properties. Similar electroosmotic flow pattern and slightly reduced particle focusing are observed in the PEO solution as compared to the Newtonian buffer, which is consistent with the observations in the constricted microchannel. The iDEP focusing and trapping of particles in the PAA solution are only available when the applied DC field is smaller than a certain threshold value. Both effects are, however, weaker than in the buffer solution, opposite to the observations in the constricted microchannel. This phenomenon may be associated with the elongation and relaxation of long PAA molecules as they are advected through the array of posts. Similar to that in the constricted microchannel, the XG solution does not exhibit an apparent iDEP effect on particles in the post-array channel. Interestingly, electroosmotic flow instability occurs under high DC electric fields in the post-array channel only.

DEDICATION

Dedicated to my Family, who are a continuous source of inspiration in every path of my life.

ACKNOWLEDGMENTS

I would like to first thank my advisor, Dr. Xiangchun Xuan, for providing me with the opportunity to work with and for him during the past two and half years. He has guided me through every aspect of my graduate studies with patience and encouragement.

In that same vein, I would like to earnestly thank Dr. Byrd, for allowing me the opportunity to assist him as a Lab assistant. Your trust in me was more instructive than I could have imagined, and your willingness to teach me was always appreciated.

I would also like to express my sincere appreciation for my friends and colleagues, Dr. Amirreza Malekanfard, Mahmud Raihan, Kuldip Bawankule, Sen Wu, Joshua Umo, Abraham Umo, Rithvik Rao, Jeremy Yang and Abhishek Saha. Thank you for your computational work, experimental expertise, and support for coursework. Without you, I would have had a much harder time in lab, class, and life. You have each taught me so much through your kindness and support.

Finally, I would like to extend my gratitude to my family and friends outside of Clemson for their constant encouragement, love, and support throughout my life.

TABLE OF CONTENTS

Page

LIST OF FIGURES

Figure Page

NOMENCLATURE

ζ_w	Wall zeta potential
ζ_P	Particle zeta potential
μ_{EO}	Electro-osmotic mobility
μ_{EP}	Electrophoretic mobility
μ_{EK}	Electrokinetic mobility
$\boldsymbol{U}_{EO}$	Electro-osmotic velocity
$\boldsymbol{U}_{EP}$	Electrophoretic velocity
$\boldsymbol{U}_{EK}$	Electrokinetic velocity
$\boldsymbol{E}$	Electric field
E_{DC}	DC Electric field
E_{AC}	AC Electric field
ε_f	Real component of fluid permittivity
μ_f	Fluid dynamic viscosity
$\boldsymbol{F}_{Elec}$	Electric field force on an arbitrary particle
q	Particle net charge
$\boldsymbol{p}$	Dipole component of force resulting from a particle in an electric field
d	Particle diameter
R	Particle radius
x	Arbitrary spatial term
$\boldsymbol{E}_{DEP}$	Theoretical dielectrophoretic component of electric field
$\boldsymbol{F}_{DEP}$	Dielectrophoretic force on an arbitrary particle

Nomenclature (Continued)

$\tilde{\varepsilon}_p$	Complex permittivity of a particle
$\tilde{\varepsilon}_f$	Complex permittivity of a fluid
σ	Conductivity
ω	Angular frequency
i	Imaginary number
f_{CM}	Claussius-Mossotti factor
σ_p	Particle conductivity
σ_f	Fluid conductivity
$RE[f_{CM}]$	Real component of the Claussius-Mossotti factor
Re	Reynolds number
El	Elasticity number
Wi	Weissenberg number
ρ	Fluid density
V	Average fluid velocity inside constriction
w_c	Constriction width
h	Microchannel height
η	Fluid viscosity
η_∞	Viscosity at infinite shear
η_o	Viscosity at zero shear rate
λ	Fluid relaxation time
γ	Shear rate

Nomenclature (Continued)

$\bar{\dot{\gamma}}$	Shear rate inside constriction
λ_{CY}	Time constant at onset of shear thinning
n	Power law index
M_w	Molecular weight
s	Streamline direction
$\mathcal{R}$	Radius of curvature of the streamline
$\hat{\mathbf{s}}$	Unit vector for streamline direction
$\hat{\mathbf{n}}$	Unit vector for normal to streamline direction
U_{DEP_s}	Dielectrophoretic particle velocity along streamline
U_{DEP_n}	Dielectrophoretic particle velocity normal to streamline
μ_{DEP}	Dielectrophoretic particle mobility
$G_D(Wi, n)$	Correction factor to account for rheological effects on traditional Stoke drag coefficient
$G_{EK}(Wi, n)$	Correction factor to account for rheological effects on electrokinetic mobility
β	Ratio of dielectrophoretic mobility to electrokinetic mobility
r	Ratio of AC to DC electric field

CHAPTER 1

INTRODUCTION

1.1 Aims and Motivation

Studies in microfluidics are becoming increasingly relevant in today's fast paced technological environment. The last few decades have seen a rapid increase in the implementation of its applications in mechanical and biomedical engineering. One of such implementations is in "Lab-on-a-chip" (LOC) devices [6,7]. The objective of this application is to reduce cost, improve effectiveness, and enhance portability by integrating one or more laboratory functions into a chip only a few square centimeters or even millimeters in size. A major advantage this presents is the availability of similar services in locations where large machines are not accessible [8]. As a result of its miniaturized nature, it is more cost efficient and environmentally friendly as lower sample volumes are required.

As research in this area advances, there has been rapid development of a variety of technologies to manipulate particles including more established methods based on microfluidics. Particle manipulation is often required in many applications such as bioanalysis, disease diagnostics, drug delivery and self-cleaning surfaces. Due to the important applications of this area, diverse means of particle manipulations are being researched into including hydrodynamic, acoustic, optics, magnetic and electrical [9]. The electrical technique is perhaps the first and most robust technique for achieving particle manipulation [10]. The transport of fluids and particles by means of an electric field is generally referred to as Electrokinesis. Recently, classical concepts under electrokinesis are used in detecting pathogens. Coupled with microfluidics for faster diagnosis, it has become increasingly relevant in facing today's challenges such as the COVID pandemic [11]. The particle manipulations in question can be discussed in three categories: separating,

focusing, and trapping of which the latter two are further discussed in this thesis. Focusing can be described as a phenomenon where synthetic or bio-particles align into a single streamline as they move. Trapping is also a form of particle concentration; however, it requires a restriction of movement from a region of the microchannel [10]. While there have been a number of studies on electrokinesis in non-Newtonian fluids [12], the vast majority of them are theoretical (or numerical), where various constitutive equations have been used to consider the fluid rheological properties [13-15]. Experimental investigations in this direction are fewer. As many of the biological (e.g., blood, saliva, DNA solutions, etc.) and chemical (e.g., polymer and colloidal solutions) fluids exhibit non-Newtonian behaviors [16], it becomes important to experimentally investigate how the fluid rheological properties may affect particle manipulation.

Thus, the objective of this study is to experimentally investigate the effects of fluid rheology on particle focusing and trapping for electric driven flow. This study will help in the design and optimization of different microfluidic systems as well as advancement in the theoretical studies of non-Newtonian fluids for modelling and simulation purposes.

1.2 Background Information on Particle Manipulation in Microfluidics

Efficient and controlled manipulation of particles is desirable in fundamental research and applications such as disease diagnostics and therapeutics [17, 18], drug discovery and delivery [19-21], and biomedical and biochemical research [22-26]. In bio-microfluidics, being able to manipulate a single particle or cell allows the observation of subtle differences among individual cells which are not discernible at a population level. The advancement of microfluidic technologies brings to bear an extensive scope of possibilities for particle manipulation in continuous flows which include transportation, separation, trapping and enrichment by utilizing

various force fields techniques. These techniques can be classified generally as passive, active or combined [27].

The passive technique makes use of interaction between the particles, microchannel structure, and the flow field. An extensively researched method under passive techniques is the Pinched Flow Fractionation (PFF) which is used for continuous sizing of particle in microchannel by employing the characteristics of laminar flow [28]. Other passive techniques include Filtration [29], Micro Hydrocyclone [30], Micro Vortex Manipulation [31], Inertia and Dean Flow Fractionation [32], Zweifach-Fung Effect [33] etc.

The active techniques which typically involves the existence of one or more external force fields which interact with the particles in distinct ways depending on the characteristics of the particle species includes hydrodynamic [34,35], acoustic [36], electrical [37, 38], optical [39], and magnetic [40,41] fields. Also, some nature inspired ideas under this technique have been proposed where non-reciprocally beating cilia act to transport fluids and particles in many biological systems [42-46] like the transportation of egg cells to the uterus by motile cilia lining the inner walls of the fallopian tubes [47,48], or the transportation of mucus and infectious agents out of the respiratory tract by motile cilia in the mammalian lung and windpipe [48,49]. Continuous flow particle manipulations may also be based on internal forces evolving from microchannel topology. Among these types are inertial microfluidics [50], hydrophoresis [51], hydrodynamic filtration [52], deterministic lateral displacement [53], insulator-based dielectrophoresis [54], etc.

Electric field forces are the most widely utilized external force fields because of their usefulness for manipulation based on a wider range of particle properties like size, charge etc. [55]. It is the force field on which this study is based.

1.3 Background on electrokinetic flow

1.3.1 Electro-osmosis

Electro-osmosis (EO) is a term used to refer to fluid flows caused under the action of an external electric field allowing for well-behaved and easily controlled streams. For electric driven flows, thin Electrical Double Layers (EDLs) form on channel walls (liquid-solid interface) resulting from counter-ions (ions of opposite charge) of aqueous solutions attracted to the opposite and intrinsically charged wall surfaces while co-ions (same charge ions) are repelled. The formed EDL consists of a closely bound compact (stern) layer and a secondary diffused layer with a net charge countering the surface charge because the number of counter-ions exceeds that of the co-ions close to the surface [56]. These counter-ions are set to motion by applying an electric field parallel to the wall. The mobile ions drag bulk liquid in the direction of the electric force resulting in electro-osmotic flow. The flow produced possesses a generally uniform velocity distribution characterized by a plug-like form unlike the conventional parabolic form in pressure driven flows [57] as illustrated in Fig. 1.1. This plug-like profile facilitates the manipulation of flow. The resulting electrical potential at the edge of the stern layer is known as the wall zeta potential (ζ_w) and serves as an approximation of the potential at the wall itself [58]. The charge of microchannel surfaces depends on the pH of introduced aqueous solution. However, for the purposes of this study, a negatively charged wall is assumed. The resulting electro-osmotic velocity $\boldsymbol{U}_{EO}$ can be expressed as follows based on [59]:

$$\boldsymbol{U}_{EO} = -\frac{\varepsilon_f \zeta_w}{\mu_f}\boldsymbol{E} = \mu_{EO}\boldsymbol{E} \tag{1.1}$$

where ε_f is the real component of fluid permittivity, μ_f is the fluid dynamic viscosity, $\boldsymbol{E}$ is the electric field and, $\mu_{EO} = -\frac{\varepsilon_f \zeta_w}{\mu_f}$ is electro-osmotic mobility.

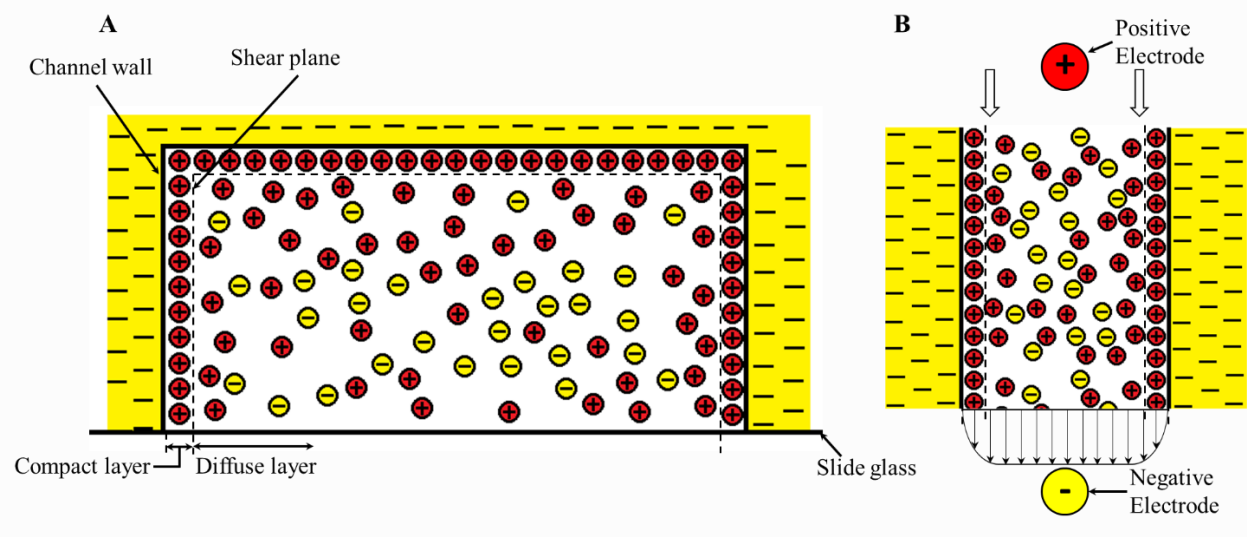

Figure 1.1 Illustrates a theoretical schematic of the electric double layer and resulting electroosmotic flow. Positively charged ions are represented as red circles, while negative ions are represented as yellow circles. Channel walls are yellow as an indication of their negative charge. The dashed line represents the interface of the compact layer and the diffuse layer. Block arrows indicate the direction of moving free counter-ions. (A) shows an elevation along the channel as viewed from the negative terminal to the positive terminal. (B) show a top view of the channel.

1.3.2 Electrophoresis

Electrophoretic motion is the movement of an electrically charged surface relative to a stationary liquid under the action of an applied external electric field [9]. By definition, it operates similar to electro-osmosis. By electrophoresis, charged particles migrate toward electrodes of opposite charge (in most cases, toward the anode [60]). Particle motion under uniform electric field results from the combination of electro-osmosis and electrophoresis. Within a uniform electric field, they define the relative motion of particles and electrolytes [61]. It has been observed in most electric driven flows that electrophoretic motion opposes electro-osmotic motion: positively charged counter-ions migrate in the direction of the electric field while negatively charged particles migrate towards the anode. However, it is worth noting that the migration of particles toward the anode is mitigated by a similar formation of EDL around them. This causes an

overpowering influence of electroosmosis on particles resulting in a net motion in the direction of fluid flow along the electric field lines [62]. The resulting particle mobility from electrophoresis and electro-osmosis is expressed as electrokinetic mobility, μ_{EK} according on Hawkins et al [59] as follows:

$$\boldsymbol{U}_{EP} = \frac{\varepsilon_f \zeta_P}{\mu_f}\boldsymbol{E} = \mu_{EP}\boldsymbol{E} \tag{1.2}$$

$$\boldsymbol{U}_{EK} = \boldsymbol{U}_{EP} + \boldsymbol{U}_{EO} = (\mu_{EP} + \mu_{EO})\boldsymbol{E} = \frac{\varepsilon_f(\zeta_P - \zeta_w)}{\mu_f}\boldsymbol{E} = \mu_{EK}\boldsymbol{E} \tag{1.3}$$

Where $\boldsymbol{U}_{EP}$ is the electrophoretic velocity, ζ_P is the zeta potential of the particle, $\mu_{EP} = \frac{\varepsilon_f \zeta_P}{\mu_f}$ is the electrophoretic mobility and $\boldsymbol{U}_{EK}$ is the electrokinetic particle velocity. The opposing signs of the component velocities conform to the priorly discussed mechanism of their flow phenomena.

1.3.3 Dielectrophoresis

Dielectrophoresis (DEP) was first investigated by Herbert Pohl in the 1950s [63]. DEP is the motion of a particle, regardless of surface charge, in response to a nonuniform (inhomogeneous) electric field (either DC or AC) as a result of the difference in polarizability between the particle and the suspending fluid. Dielectrophoretic force is a function of the spatial electric field gradient an independent of the direction of applied electric field [64]. Particles are caused to move toward the higher (positive dielectrophoresis (pDEP)) or lower electric field intensities regions (negative dielectrophoresis (nDEP)) depending on the relative permittivity of particles with respect to the surrounding fluid. Particles with relatively higher permittivity are more polarizable in comparison with the surrounding fluid and will undergo pDEP whereas particle with relatively lower permittivity are less polarizable and will undergo nDEP. The strength of

the force from dielectrophoresis depends on the dielectric properties of both the surrounding medium and the particle, on particle shape and size and on the frequency of the applied electric field [39]. Dielectrophoresis is widely used for particle trapping [65,66], focusing [1], separation [67] and exchange or washing [68]. An induced potential similar to an induced dipole is generated with a particle suspended in fluid is subjected to an electric field. The force experienced by the particle ($\boldsymbol{F}_{Elec}$) due to the electric field can be expressed as:

$$\boldsymbol{F}_{Elec} = q\boldsymbol{E} + \boldsymbol{p}.\boldsymbol{\nabla}\boldsymbol{E} + \cdots \tag{1.4}$$

where q is the particle net charge and $\boldsymbol{p}$ is the dipole force component [69]. For a field of uniform electric field ($\boldsymbol{\nabla}\boldsymbol{E} = 0$), the higher order terms vanish, leaving only the Coulombic interaction force, $q\boldsymbol{E}$. However, the presence of the particle generates nonuniformity in the electric field causing dielectrophoretic component to persist. Eq. (1.4) is generated from a Taylor series expansion, Eq. (1.5) of the electric field, $\boldsymbol{E}(x + d)$ about an arbitrary point, for a particle diameter, $d = 2R$, where R is the particle radius.

$$\boldsymbol{E} = \boldsymbol{E}(x) + 2R \cdot \frac{\partial \boldsymbol{E}}{\partial x} + \cdots + \frac{(2R)^n}{(\boldsymbol{n}!)} \cdot \frac{\partial^n \boldsymbol{E}}{\partial x^n} + \cdots \tag{1.5}$$

In cases where particle diameters are sufficiently small against electric field nonuniformity, the second term of the expansion is a suitable approximation of the dielectrophoretic component under consideration, $\boldsymbol{E}_{DEP}$.The dielectrophoretic force, $\boldsymbol{F}_{DEP}$, as defined by the second term of Eq. 4 can subsequently be expressed as:

$$\boldsymbol{F}_{DEP} = \boldsymbol{p}.\boldsymbol{\nabla}\boldsymbol{E} = \boldsymbol{p}.2R \cdot \frac{\partial \boldsymbol{E}}{\partial x} \tag{1.6}$$

for

$$\boldsymbol{p} = 4\pi\varepsilon_f R^3 \left(\frac{\tilde{\varepsilon}_p - \tilde{\varepsilon}_f}{\tilde{\varepsilon}_P + 2\tilde{\varepsilon}_f}\right)\boldsymbol{E} \tag{1.7}$$

Where $\tilde{\varepsilon}_p$ and $\tilde{\varepsilon}_f$ are the complex permittivity of the particle and fluid, respectively. From a broad perspective, permittivity according to Morgan et al [70] can be expressed as:

$$\tilde{\varepsilon} = \varepsilon - i\frac{\sigma}{\omega} \tag{1.8}$$

Where σ is the conductivity, i is the imaginary number, and ω is the angular frequency. Depending on conditions of the electric field, the Classius-Mossotti (CM) factor, f_{CM}, which is the term in parentheses in Eq. 7 can be simplified substantially. The Classius-Mossotti relation connects the relative permittivity of a dielectric to the polarizability of the atoms or molecules constituting the dielectric. For Direct Current (DC) fields and low frequency Alternating Current (AC), the CM factor becomes:

$$f_{CM} = \frac{\sigma_p - \sigma_f}{\sigma_p + 2\sigma_f} \tag{1.9}$$

Such that $\boldsymbol{F}_{DEP}$ can be reduced to Eq. 1.10.

$$\boldsymbol{F}_{DEP} = 2\pi\varepsilon_f R^3 RE[f_{CM}](\boldsymbol{\nabla}\boldsymbol{E}^2) \tag{1.10}$$

Where $RE[f_{CM}]$ represents the real component of the Classius-Mossotti (CM) factor.

1.4 Background Information on Non-Newtonian fluids and Rheology

Classical fluid mechanics were developed for Newtonian fluids. However, the past few decades have seen rapid development in the theory of non-Newtonian fluid dynamics. In a broad sense, fluids can be categorized as Newtonian and non-Newtonian fluids. Newtonian fluids obey Newton's law of viscosity and possess a constant viscosity independent of shear stress unlike

non-Newtonian fluids for which viscosity vary. This categorization of fluids is generally represented by a rheological model or correlation of shear stress and shear rate. Whereas the relationship between shear stress and shear rate for Newtonian fluids is linear, this relationship is non-linear for non-Newtonian fluids. There is a growing importance in the study of non-Newtonian fluid mechanics for fields concerned with materials whose flow behaviors cannot be characterized by Newton's law of viscosity.

Skelland (1967) generally classifies non-Newtonian fluids into three groups according to the relationship between shear stress and shear rate: (1) time-independent non-Newtonian fluids; (2) time-dependent non-Newtonian fluids; and (3) viscoelastic non-Newtonian fluids. Time-independent non-Newtonian fluids present shear rates unique but non-linear functions of the instantaneous shear stress at that point. For time-dependent non-Newtonian fluids, the shear rate does not only depend on the shear stress but also on the shearing time or on the previous shear stress rate history of the fluid. Viscoelastic non-Newtonian fluids exhibit both elastic and viscous properties and show partial recovery upon the removal of the shear stress. This implies that the rheological properties will not only depend the shear rate and shear stress relationship but also on the recent history of the material [71]. Another way of classifying non-Newtonian fluids is based on their flow behavior with regards to increasing or decreasing viscosities with applied shear stress. Those who exhibit increasing viscosities with shear stress are referred to as shear-thickening fluids whereas fluids which exhibit decreasing viscosities with shear stress are referred to as shear-thinning fluids (See Fig. 1.2) This study is based on the non—Newtonian fluid with characteristics of the latter category.

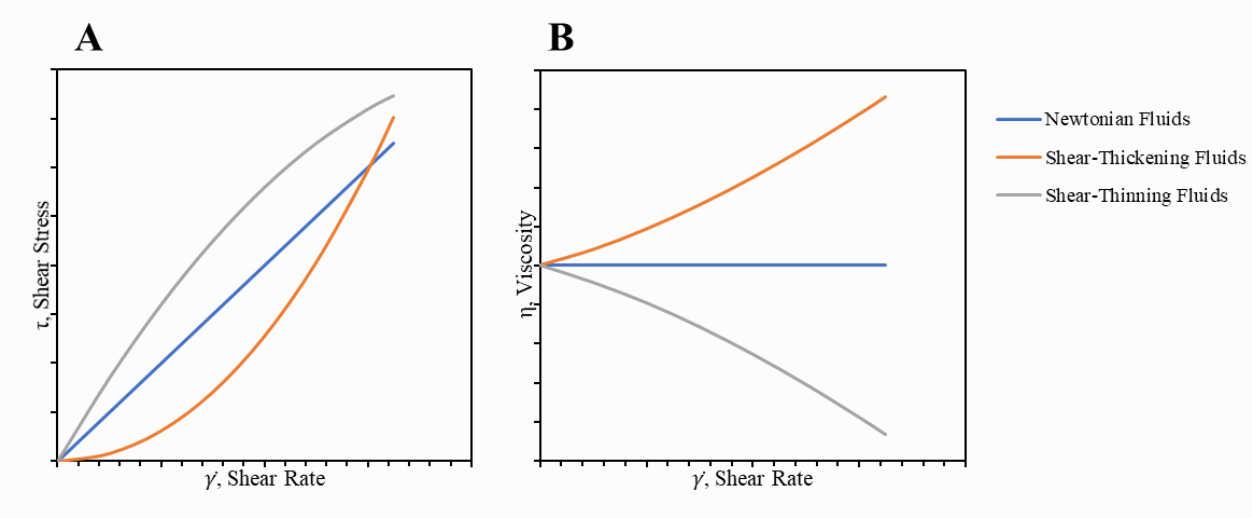

Figure 1.2 (A) Represents a typical shear stress and shear rate relationship for Newtonian and non-Newtonian fluids. (B) Represents a typical viscosity and Shear rate relationship for Newtonian and non-Newtonian fluids.

Fluid rheological properties are derived from the rheological model and are used to characterize the specific way in which flow behaviors occur. [72]. For the purpose of this thesis, two rheological properties are considered in the analysis and discussion of results obtained from the experiments which are shear-thinning and elasticity. Shear thinning is characterized by the power law index, *n,* which is a dimensionless number. Note that $n = 1$ indicates a Newtonian of Boger (i.e purely elastic [73]) fluid. Values of $n < 1$, indicate shear thinning effect (weakly shear thinning if $1 > n \geq 0.65$ [74]) The fluid elasticity effect is characterized by the elasticity number, El, which is a ratio of the Weissenberg number, Wi, to the Reynolds number, Re [75] and is expressed as following:

$$Re = \frac{2\rho V w_c h}{\eta(w_c + h)} \tag{1.11}$$

$$Wi = \lambda\bar{\dot{\gamma}} = \frac{2\lambda V}{w_c} \tag{1.12}$$

$$El = \frac{Wi}{Re} = \frac{\lambda\eta(w_c+h)}{\rho {w_c}^2 h} \quad (1.13)$$

in which, ρ is the fluid density, V is the average fluid velocity inside constriction, w_c is the constriction width, h is the microchannel height, η is fluid viscosity, $\bar{\dot{\gamma}} = \frac{2V}{w_c}$ is the shear rate, and λ is the fluid relaxation time.

The variation of shear thinning fluids with shear rate is determined using the Carreau model:

$$\frac{\eta-\eta_\infty}{\eta_o-\eta_\infty} = [1 + (\lambda_{CY}\bar{\dot{\gamma}})^2]^{(n-1)/2} \quad (1.14)$$

where, η_∞ is the viscosity at infinite shear rate, η_o is the viscosity at zero shear rate, λ_{CY} is a time constant at onset of shear thinning (inverse of shear rate at the onset of shear thinning), n is the power law index. The constant 2 is used as the fitting parameter based on the Carreau model. Viscosities for the fluids used in this study vary with shear rate (γ) are obtained using a rheometer.

1.5 Thesis Overview

The objective of this thesis is to experimentally determine rheological properties of non-Newtonian fluids that affect dielectrophoretic particle trapping and focusing in broad terms based on an understanding of how these rheological properties affect electro-osmotic flow patterns. The first experiment (chapter 2) involves a single constriction channel. This simple microchannel geometry allows for fundamental understanding of the phenomena involved with the study. The experiment is run on three non-Newtonian solution with polymer base concentrations that produce distinct rheological properties. Electro-osmotic and electrokinetic results from these solutions are compared to that from a Newtonian solution. This way a substantive conclusion is

made on which rheological properties enhanced or diminished dielectrophoretic effects for trapping and focusing of particles.

A similar experiment is run in a post-array channel (chapter 3) which presents a relatively more complex geometry. Polymer structure is expected to play a role directly affecting electro-osmotic flow pattern. Consequently, the resulting particle mobility which theoretically is a resultant from electroosmosis, electrophoresis and dielectrophoresis should be influenced.

1.6 References

[1] Xuan, X., *Electrophoresis* 2019, *40,* 2484–2513.

[2] Ko, C. H., Li, D., Malekanfard, A., Wang, Y. N., Fu, L. M., Xuan, X., *Electrophoresis* 2019, *40*, 1387–1394.

[3] Li, D., *Electrokinetics in Microfluidics.* Elsevier Academic Press, Burlington 2004.

[4] Chang, H. C., Yeo, L. Y., *Electrokinetically Driven Microfluidics and Nanofluidics*. Cambridge University Press, New York 2010.

[5] Ramos, A., *Electrokinetics and Electrohydrodynamics in Microsystems.* Springer, Berlin 2011.

[6] Malic, L., Brassard, D., Veres, T., Tabrizian, M., *Lab Chip,* 2010,10, 418-431.

[7] Arshavsky-Graham S., Segal E., *Lab-on-a-Chip Devices for Point-of-Care Medical Diagnostics. In:. Advances in Biochemical Engineering/Biotechnology*. Springer, Berlin, Heidelberg 2020.

[8] Xuan, X., Electrophoresis 2008, 298, 33–43.

[9] Zhang, S., Wang, Y., Onck, P. R., den Toonder, J., Microfluid. Nanofluid. 2020, 24, 24.

[10] DuBose, J., "ELECTROKINETIC PARTICLE MANIPULATIONS IN SPIRAL MICROCHANNELS" (2014). *All Theses.* 1969.

[11] Bhalla, N., Pan, Y., Yang, Z., Payam, A. F., *ACS Nano* 2020, 14, 7, 7783–7807.

[12] Zhao, C., Yang, C., *Adv. Colloid. Interf. Sci.* 2013, *201–202*, 94–108.

[13] Zhao, C., Yang, C., *Biomicrofluidics* 2011, *5*, 014110.

[14] Mei, L., Zhang, H., Meng, H., Qian, S., Micromachines 2018, 9, 155.

[15] Mei, L., Qian, S., Micromachines 2019, 10, 747.

[16] Bird, R. B., Armstrong, R. C., Hassager, O., Dynamics of Polymeric Liquids, Willey, vol.1, 1977.

[17] Gossett, D. R., Weaver, W. M., Mach, A. J., Hur, S. C., Tse, H. T., Lee, W., et al., *Analytical and Bioanalytical chemistry*, 2010, 397(8), 3249-3267.

[18] Puri, I. K., Ganguly, R*., Annual Review of Fluid Mechanics*, 2013, Vol. 46:407-440.

[19] Dittrich, P., Manz, A., *Nature Reviews Drug Discovery*, 2006, vol. 5, 210–218.

[20] Kang, Y., Li, D., Kalams, S. A., & Eid, J. E. *Biomedical Microdevices,* 2008 10(2), 243-249.

[21] Nguyen, N.-T., Wu Z., *J. Micromech. Microeng.* 2004, 15 R1

[22] Pamme, N., *Lab on a Chip,* 2007, 7(12), 1644-1659.

[23] Ateya, D. A., Erickson, J. S., Howell Jr, P. B., Hilliard, L. R., Golden, J. P., Ligler, F. S., *Analytical and Bioanalytical Chemistry,* 2008, vol 391, pages1485–1498.

[24] Nilsson, J., Evander, M., Hammarström, B., Laurell, T., *Analytica Chimica Acta,* 2009, 649 141–157.

[25] Xuan, X., Zhu, J., Church, C., *Microfluidics and Nanofluidics*, 2010, 9(1), 1-16.

[26] Karimi, A., Yazdi, S., Ardekani, A. M., *Biomicrofluidics,* 2013, 7, 021501.

[27] Sajeesh, P., Sen A. K., *Microfluidics and Nanofluidics,* 2014,17, 1–52.

[28] Yamada, M., Nakashima, M., Seki, M., *Anal. Chem.* 2004, 76, 5465-5471.

[29] Sugaya, S., Yamada, M., Seki, M., *Biomicrofluidics,* 2011 5 (2) 24103

[30] Bhardwaj, P., Bagdia, P., Sen, A. K*., Lab Chip,* 2011,11, 4012-4021

[31] Collins, D. J., Ma, Z., Han, J., Ai, Y., *Lab Chip,* 2017, 17, 91-103

[32] Johnston, I. D., McDonnell, M. B., Tan, C. K. L., McCluskey, Davies, D. K., Tracey, M. C., *Microfluidics and Nanofluidics*, 2014, 17, 509–518.

[33] Doyeux, V., Podgorski, T., Peponas, S., Ismail, M., Coupier. G., *2nd European Conference on Microfluidics,* 2010, pp.1-17, Toulouse, France.

[34] Vig, A. L., & Kristensen, A., *Applied Physics Letters,* 2008, 93(20), 203507.

[35] Takagi, J., Yamada, M., Yasuda, M., & Seki, M., *Lab on a Chip,* 2005, 5(7), 778-784.

[36] Laurell, T., Peterssona, F., Nilssona, A., *Chem. Soc. Rev.,* 2007, 36, 492-506.

[37] Zhang, C.-X., Manz, A., *Analytical Chemistry*, 2003, 75(21), 5759-5766.

[38] Gascoyne, P. R., Vykoukal, J., *Electrophoresis,* 2002, 23(13), 1973-1983.

[39] Lenshof, A., Laurell, T., *Chem. Soc. Rev*., 2010, 39, 1203-1217.

[40] Liang, L., Zhang, C., & Xuan, X., *Applied Physics Letters,* 2013, 102(23), 234101.

[41] Pamme, N., *Lab on a Chip,* 2006, 6(1), 24-38.

[42] Kim, J., Kang, S., Lee, B., Ko, H., Bae, W.-G., Suh, K. Y., Kwak, M. K., Jeong, H. E., *Sci Rep*, 2015, 5, 17843.

[43] Ben, S., Tai, J., Ma, H., Peng, Y., Zhang, Y., Tian, D., Liu, K., Jiang, L., *Adv. Funct. Mater.* 2018, 28, 1706666.

[44] Lin, Y., Hu, Z., Zhang, M., Xu, T., Feng, S., Jiang, L., Zheng, Y., Adv. Funct. Mater. 2018, 28, 1800163.

[45] Yang, Z., Park, J. K., Kim, S., *Small*, 2018, 14, 1702839.

[46] Zhang, S., Wang, Y., Onck, P. R., den Toonder, J., *Adv. Funct. Mater.* 2019, 29, 1806434.

[47] Fauci, L., Dillon, R., *Annual Review of Fluid Mechanics*, 2006, Vol. 38:371-394.

[48] Enuka, Y., Hanukoglu, I., Edelheit, O., Vaknine, H., Hanukoglu, A., *Histochem Cell Biol*, 2012, 137, 339–353.

[49] Sleigh, M. A., *Camp. Biochem. Physiol*., 1989, Vol. 94A. No. 2. pp. 359-364.

[50] Di Carlo, D., *Lab on a Chip,* 2009, 9(21), 3038-3046.

[51] Choi, S., Song, S., Choi, C., Park, J.-K., *Analytical Chemistry*, 2009, 81(5), 1964-1968.

[52] Yamada, M., Seki, M., *Lab on a Chip*, 2005, 5(11), 1233-1239.

[53] Huang, L. R., Cox, E. C., Austin, R. H., Sturm, J. C., *Science,* 2004, 304(5673), 987-990.

[54] Srivastava, S. K., Gencoglu, A., Minerick, A. R., *Analytical and Bioanalytical Chemistry*, 2011, 399(1), 301-321.

[55] Zhu, J., Xuan, X., *Biomicrofluidics*, 2011, 5(2), 024111.

[56] Kang, Y., Li, D., *Microfluidics and Nanofluidics,* 2009, 6(4), 431-460.

[57] Hsieh, S.-S., Lin, H.-C., Lin, C.-Y., *Colloid Polym Sci.* 2006; 284(11): 1275–1286.

[58] Karniadakis, G., Beskok, A., & Aluru, N., *Microflows and Nanoflows: Fundamentals and Simulation,* 2005, New York: Springer Science+Business Media.

[59] Hawkins, B. G., Smith, A. E., Syed, Y. A., Kirby, B. J., *Analytical Chemistry,* 2007, 79(19), 7291-7300.

[60] Masliyah, J. H., Bhattacharjee, S., *Electrokinetic and Colloid Transfer Phenomena,* 2006, Hoboken: John Wiley & Sons, Inc.

[61] Levine, S., Neale, G. H., *Journal of Colloid and Interface Science,* 1974, 47(2), 520-529.

[62] Santiago, J. G., *Analytical Chemistry,* 2001, 73(10), 2353-2365.

[63] Pohl, H. A., *Journal of Applied Physics,* 1951, 22(7), 869-871.

[64] Hughes, M. P., *Electrophoresis,* 2002, 23(16), 2569–2582.

[65] Cummings, E. B., Singh, A. K., *Analytical Chemistry*, 2003, 75(18), 4724-4731.

[66] Gadish, N., Voldman, J., *Anal. Chem.*, 2006, 78, 22, 7870–7876.

[67] Adams, J. D., Kim, U., Tom Soh, H., *PNAS,* 2008 105 (47) 18165-18170.

[68] Tornay, R., Braschier T., Demierre, N., Steitz, B., Finka, A., Hofmann, H., Hubbell, J. A. Renaud, P., *Lab Chip,* 2008,8, 267-273.

[69] Gascoyne, P. R., Vykoukal, J., *Electrophoresis,* 2002, 23(13), 1973-1983.

[70] Morgan, H., Sun, T., Holmes, D., Gawad, S., Green, N. G., *Journal of Physics D: Applied Physics,* 2007, 40(1), 61-70.

[71] Wu, Y. S., *Lawrence Berkeley Laboratory,* 1990, Ph.D Thesis.

[72] Figura, L. O., Teixeira, A. A., *Rheological Properties. In: Food Physics,* 2007, Springer, Berlin, Heidelberg.

[73] James, D. F., Annu. Rev. Fluid Mech. 2009, 41, 129–142.

[74] Lindner, A., Bonn, D., Meunier, J*., Phys. Fluids* 2000, 12, 256–261.

[75] Rodd, L. E., Scott, T. P., Boger, D. V., Cooper-White, J. J., McKinley, G. H., J. *Non-Newton. Fluid Mech*. 2005, 129, 1–22.

CHAPTER 2

INSULATOR-BASED DIELECTROPHORETIC FOCUSING AND TRAPPING OF PARTICLES IN NON-NEWTONIAN FLUIDS IN A CONSTRICTION MICRO-CHANNEL.

2.1 Background on DEP in Constriction Micro-channel.

Microfluidic manipulation of particles and cells is a rapidly developing area that facilitates solving challenges in the fields of analytical chemistry, bioanalysis, cell biology and clinical applications [1,2]. It has been implemented through both passive (e.g., flow induced-inertial [3-5] and elastic [6-8]) and active (e.g., externally imposed acoustic [9,10], magnetic [11,12] and optical [13]) force fields. Insulator-based dielectrophoretic (iDEP) microdevices use insulating structures to create electric field gradients for continuous-flow focusing [14,15], trapping [16,17], patterning [18], concentration [19,20], poration [21], and separation [22-24] of particles and cells. They have, however, been limited to work with Newtonian fluids in the majority of the reported applications [25-27]. As many of the biological (e.g., blood, saliva, DNA solutions, etc.) and chemical (e.g., polymer and colloidal solutions) fluids exhibit non-Newtonian behaviors [28-30], it becomes important to understand how the fluid rheological properties may affect the iDEP focusing and trapping of particles.

There have been a number of studies on fluid electroosmosis and particle electrophoresis in non-Newtonian fluids through microchannels [31]. However, the vast majority of them are theoretical (or numerical), where various constitutive equations have been used to consider the fluid rheological properties [32-42]. Experimental investigations in this direction are much less. For the electroosmotic fluid flow, drag reduction was reported in viscoelastic polyethylene glycol [43], polyacrylamide (PAA) [44], and polyethylene oxide (PEO) [45,46] solutions because of the wall-depletion layer and/or fluid shear thinning effect. Elastic instabilities were observed in the

electroosmotic flow of PAA solution through both a constricted [47,48] and a cross-shaped [49] microchannel when the imposed DC electric field reaches a threshold value. They were also numerically studied [50,51]. Our group has recently performed an experimental study of the sole and combined effects of fluid elasticity and shear thinning on the electroosmotic flow of polymer solutions in a constricted microchannel [52]. Fluid shear thinning was observed to cause flow circulations in the shear-thinning xanthan gum (XG) solution while fluid elasticity tends to stabilize the flow of polyvinylpyrrolidone (PVP), PEO and PAA solutions.

Our group has also conducted experiments on particle electrophoresis in non-Newtonian fluids. Polystyrene particles in the electroosmotic flow of XG solution were observed to migrate towards the walls in a straight rectangular microchannel, opposite to the centerline focusing effect in a Newtonian fluid [53]. The electrophoretic slip tuned particle migration in an electro-hydrodynamic flow of PEO solution was found either opposite to [54] or in the same direction [55] as that in a Newtonian fluid, depending on the polymer concentration. These observations were explained by theoretical [55,56] and numerical [57] analyses. In addition, an unexpected oscillation was observed for particles travelling along with the electroosmotic flow of PEO solutions in a constricted microchannel [58]. It is, however, absent from particles traveling against the electroosmotic flow, which experience a defocusing effect with the increase of DC electric field [59]. We present in this work an experimental study of particle electrophoresis in three types of non-Newtonian fluids with distinct rheological properties through the same constricted microchannel. Our aim is to obtain an improved understanding of how the fluid elasticity and/or shear thinning affect the iDEP focusing and trapping of particles.

2.2 Experiment

2.2.1 Experimental Setup

As viewed from the picture in Fig. 2.1A, the device contains a 1 cm-long straight constricted microchannel with the main width and depth of 400 μm and 40 μm, respectively. The two-dimensional widthwise constriction is located in the middle of the channel and has a 200 μm length with a width of 40 μm.

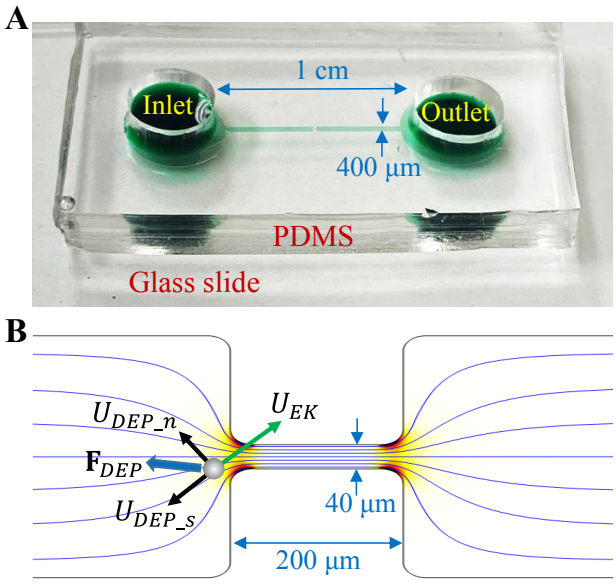

Figure 2.1 (A) Picture of the fabricated microfluidic chip where the constricted microchannel and reservoirs are filled with green food dye for clarity; (B) Illustration of iDEP focusing and trapping of particles in the constriction region of the microchannel, where the electric field gradient-induced dielectrophoretic force, $\boldsymbol{F}_{DEP}$, drives both a cross-stream particle motion, U_{DEP_n}, for focusing, and a streamwise particle motion, U_{DEP_s}, for trapping because it opposes the electrokinetic particle motion, U_{EK}. The background shows the electric field lines and the contour for the gradient of electric field squared, $\nabla \boldsymbol{E}^2$ (the darker the larger magnitude).

Polystyrene particles of 10 μm diameter (Sigma-Aldrich) were used to demonstrate the iDEP focusing and trapping. They were re-suspended into three types of non-Newtonian fluids that were each prepared in 1 mM phosphate buffer: (1) viscoelastic 1000 ppm PEO solution ($M_w = 2$ MDa, Sigma-Aldrich); (2) shear-thinning 1000 ppm xanthan gum (XG) solution (Tokyo

Chemical Industry); (3) viscoelastic and shear-thinning 100 ppm PAA solution ($M_w = 18$ MDa, Polysciences). The particle suspension in pure buffer solution was also tested as the control. Tween 20 (0.5% v/v, Fisher Scientific) was added to each prepared particle suspension for suppressing the particle-wall adhesions. The viscosities of the particle-free non-Newtonian fluids were acquired from a cone-plate rheometer (Anton Paar, MCR 302, Graz, Austria) and are presented in Fig. 2.2. Other important rheological properties are summarized in Table 2.1. Fluid electric conductivities are experimentally measured. The electric conductivity of 10 μm polystyrene particles was estimated as 4 μS/cm from the recommended surface conductance of 1 ns [69]. The relaxation time, λ, of the PEO solution was obtained directly from Rodd et al. [65]. The relaxation time of the XG solution was assumed negligible based on Lindner et al. [66]. The relaxation time of the PAA solution was calculated from the reported value of 95 ms for 200 ppm PAA solution in Poole and Escudier [67] using the following concentration scaling [68],

$$\lambda \propto c^{0.76} \tag{2.1}$$

where c is the polymer concentration.

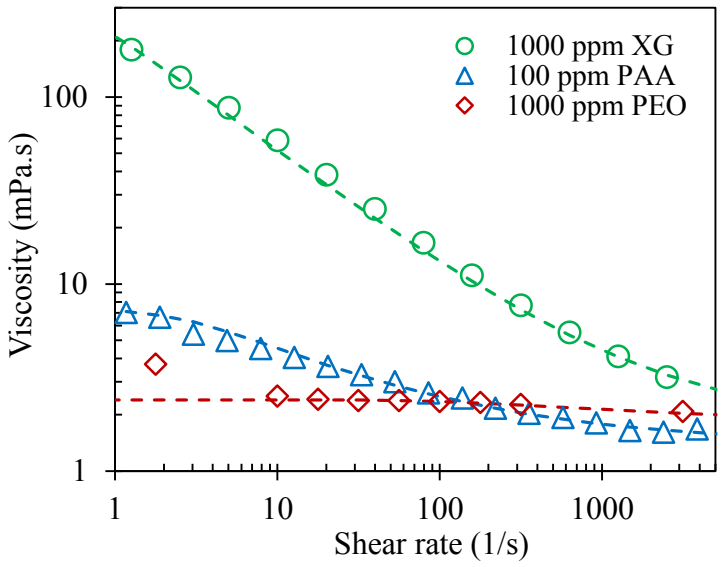

Figure 2.2 Experimentally measured viscosity data (symbols) of the prepared non-Newtonian fluids, where the dashed lines show the Carreau model-fitting.

Table 2.1. Rheological properties and Weissenberg number for the prepared fluids at 24 °C. The viscosity values, η, for the fluids with $n < 1$ were obtained using the Carreau model fitting of the measured data based on the electrokinetic particle velocity, U_{EK}, inside the constriction under 200 V DC voltage. The positive electrokinetic mobility, U_{EK}/E_{DC}, indicates that particles travel along with the DC electric field.

Solution	σ_f (μS/cm)	λ (ms)	η (mPa•s)	n	Wi	U_{EK}/E_{DC} ($\times 10^{-8}$ m^2/V·s)
Buffer	190	0	1.0	1	0	+2.0
1000 ppm PEO	196	1.5	2.34	0.85	0.2	+1.2
1000 pm XG	250	~0	9.42	0.36	~0	−1.9
100 ppm PAA	223	56.1	2.24	0.54	10.1	+1.8

2.2.2 Device Fabrication

The single constriction micro-channels were fabricated using a standard soft lithography technique. For the experiments, this technique comprises of a mold made up of a photoresist whose shape and form were adapted by a polymer material, Polydimethylsiloxane (PDMS). PDMS is a biocompatible, transparent, and inexpensive material. The photoresist mold took the shape of the transparent area of a prepared photomask. The photomask was prepared by printing the specific geometry drawn using AutoCAD® software on a photomask sheet. Glass slides were thoroughly cleaned and uniformly coated with Photoresist (SU-8 25, MicroChem Corp, Newton, MA) up to a specific depth of 40 μm utilizing a programmed spin-coater (WS-400E-NPP-Lite, Laurell Technologies, North Wales, PA). Each coated slide underwent a two-step pre-bake process: 65°C for 3 minutes and 95°C for 7 minutes on two hotplates (HP30A, Torrey Pines Scientific, San Marcos, CA). The prepared photomask was layered above the photoresist coating on the slide and exposed to UV treatment to create a negative photoresist which adapts the shape of the printed geometry on the photomask. UV intensity and exposure time were specific to the desired depth. Subsequently, the exposed slide underwent a two-step post-bake process: 65°C for 1 minute and finally 95°C for 3 minutes. The slides were then developed in an SU-8 developing

solution for 5 minutes to dissolve the positive photoresist material rinsed with the finished microchannel mold.

Dried slides with photoresist mold are placed in petri dishes and covered with PDMS. A vacuum chamber (13-262-280A, Fisher Scientific, Fair Lawn, NJ) is used to get rid of bubbles which may have been created during the preparation and depositing of the PDMS for 15 minutes. The PDMS is cured for two hours in a gravity convection oven (13-246-506GA, Fisher Scientific, Fair Lawn, 21 NJ) at 70°C. Afterwards, the petri dish is removed from the oven and allowed to cool. A scalpel is used to cut and peel the PDMS off the molds. Channel inlet and outlet were perforated using a punch of 3/8" diameter to serve as reservoirs. Clean glass slides were plasma treated for 1 minute 30 seconds after which the PDMS parts are immediately bonded to the slides on the face of the channel impression to produce the microfluidic devices.

2.2.3 Methods

The prepared particle suspensions were driven through the constricted microchannel using DC or DC-biased AC electric fields that were supplied by a function generator (33220A, Agilent Technologies) and a high-voltage amplifier (609E-6, Trek). DC voltages of up to 300 V were first applied. If no particle focusing or trapping was achieved, DC-biased AC voltages with a total root-mean-square (RMS) magnitude of 300 V were then used for enhanced iDEP effects. The average electric field through the microchannel was thus limited to a maximum of 300 V/cm across the 1 cm long microchannel. Particle motion in the constriction region was recorded using a microscope (Nikon Eclipse TE2000U, Nikon Instruments) equipped with a CCD camera (Nikon DS-Qi1Mc). The captured images were processed using the Nikon imaging software (NIS-Elements AR 2.30). The electrokinetic mobility of particles was determined using the

particle tracking velocimetry under 100 V DC voltage. Only particles traveling along the channel centerline at a sufficient distance away from the constriction were tracked. Small fluorescent particles of 0.5 μm diameter (Bangs Laboratories) were seeded into the prepared non-Newtonian fluids to visualize the electroosmotic flow pattern in the constriction region under 100 V DC.

2.3 Theory

2.3.1 Dielectrophoresis in non-Newtonian fluids

The insulating walls of the microchannel squeeze the electric field lines in the constriction region as viewed from Fig. 2.1B. Thus, electric field gradients are created locally (see the contour for the gradient of electric field squared in Fig. 2.1B), leading to a repulsive dielectrophoretic force, $\mathbf{F}_{DEP}$, acting on the suspended particle [26],

$$\mathbf{F}_{DEP} = -\pi R^3 \varepsilon \nabla \mathbf{E}^2 = -\pi R^3 \varepsilon \left(\frac{\partial \mathbf{E}^2}{\partial s} \hat{\mathbf{s}} + 2 \frac{\mathbf{E}^2}{\mathcal{R}} \hat{\mathbf{n}} \right) \tag{2.2}$$

where R is the particle radius, ε is the fluid permittivity, $\mathbf{E}$ is the electric field, s denotes the streamline direction with $\hat{\mathbf{s}}$ being its unit vector, $\mathcal{R}$ is the radius of curvature of the streamline, and $\hat{\mathbf{n}}$ is the unit vector in the direction normal to the streamline. Note that we set in Eq. 2.2 the so-called Clausius-Mossotti factor to −0.5 considering the electric conductivities of the prepared fluids (see Table 2.1) are all much larger than that of the particles. Owing to the electric origin in nature, $\mathbf{F}_{DEP}$ is independent of the fluid rheology. However, the resulting dielectrophoretic particle motion, $\mathbf{U}_{DEP}$, becomes a function of the fluid elasticity and shear thinning as these rheological properties have been each demonstrated to affect the drag force on particles in non-Newtonian fluids [60],

$$\mathbf{U}_{DEP} = -\frac{R^2 \varepsilon}{6\eta G_D(Wi,n)} \left(\frac{\partial \mathbf{E}^2}{\partial s} \hat{\mathbf{s}} + 2 \frac{\mathbf{E}^2}{\mathcal{R}} \hat{\mathbf{n}} \right) = U_{DEP\_s} \hat{\mathbf{s}} + U_{DEP\_n} \hat{\mathbf{n}} \tag{2.3}$$

$$U_{DEP\_s} = \frac{\mu_{DEP}}{G_D(Wi,n)} \frac{\partial \mathbf{E}^2}{\partial s}, U_{DEP\_n} = \frac{2\mu_{DEP}}{G_D(Wi,n)} \frac{\mathbf{E}^2}{\mathcal{R}} \tag{2.4}$$

where η is the fluid viscosity, U_{DEP_s} and U_{DEP_n} are the dielectrophoretic particle velocities along and normal to the streamline, respectively (see Fig. 2.1B), and $\mu_{DEP} = -R^2\varepsilon/6\eta$ is the dielectrophoretic particle mobility in Newtonian fluids. We introduce a correction factor, $G_D(Wi,n)$, account for the fluid rheological effects on the traditional Stokes drag coefficient in Newtonian fluids, where Wi is the Weissenberg number for the elasticity effect and n is the power-law index for the shear thinning effect,

$$Wi = \lambda\bar{\dot{\gamma}} = \frac{2\lambda V}{w_c} \tag{2.5}$$

Here, λ is the fluid relaxation time, and $\bar{\dot{\gamma}} = 2V/w_c$ is the average shear-rate inside the constriction with V being the local electric field-dependent fluid velocity and w_c the constriction width.

2.3.2 iDEP focusing and trapping

The cross-stream component of the dielectrophoretic velocity, U_{DEP_n}, competes with the streamwise electrokinetic velocity, U_{EK}, yielding a particle focusing effect towards the centerline of the microchannel (see Fig. 2.1B). Analogous to particle electrokinetics in Newtonian fluids under the thin electric double layer limit [61], U_{EK} in non-Newtonian fluids may be still viewed as the addition of fluid electroosmosis, U_{EO}, and particle electrophoresis, U_{EP},

$$U_{EK} = U_{EO} + U_{EP} = G_{EK}(Wi,n)\mu_{EK}E_{DC} \tag{2.6}$$

where $G_{EK}(Wi,n)$ denotes the correction factor for the electrokinetic mobility, $\mu_{EK} = \varepsilon(\zeta_p - \zeta_w)/\eta$, as traditionally defined for Newtonian fluids with ζ_p and ζ_w being the particle and wall zeta potentials, and E_{DC} is the DC component of the electric field. Note we have assumed an identical correction factor for fluid electroosmosis and particle electrophoresis to simplify the treatment considering their reciprocal relationship in Newtonian fluids [31]. The iDEP focusing effect is measured by the particle velocity ratio,

$$\frac{U_{DEP\_n}}{U_{EK}} = \frac{1}{G_D(Wi,n)G_{EK}(Wi,n)} \frac{2\beta(1+r^2)E_{DC}}{\mathcal{R}} \tag{2.7}$$

where $r = E_{AC}/E_{DC}$ is the AC to DC field ratio (or equivalently, the RMS voltage ratio), and $\beta = \mu_{DEP}/\mu_{EK} = R^2/6(\zeta_p - \zeta_w)$ is the particle's dielectrophoretic to electrokinetic mobility ratio that is independent of fluid rheological properties. For easy references hereafter, we term $(1 + r^2)E_{DC}$ the effective electric field. The second fraction term on the right-hand side of the equation characterizes the iDEP focusing effect for particles in Newtonian fluids [26], and the first fraction term may become more or less than unity depending on the fluid rheological effects. The streamwise component of the dielectrophoretic velocity, U_{DEP_s}, can counter-balance the electrokinetic velocity, U_{EK}, yielding a particle trapping effect, for which the threshold for the effective electric field is given by,

$$(1 + r^2)\frac{\partial E_{DC}}{\partial s} = G_D(Wi,n)G_{EK}(Wi,n)\frac{1}{2\beta} \tag{2.8}$$

Note the fraction term on the right-hand side characterizes the iDEP trapping of particles in Newtonian fluids [26].

As viewed from Eqs. (2.7) and (2.8), the fluid rheological effects on iDEP focusing and trapping of particles are both characterized by the two multiplying correction factors, i.e.,

$G_D(Wi,n)G_{EK}(Wi,n) > 1$ causes a reduction while $G_D(Wi,n)G_{EK}(Wi,n) < 1$ enhances. To simplify the analysis in the results section, we further assume the wall and particle zeta potentials are both independent of the polymer addition, which is common in the theoretical analysis [31-42]. Thus, the particle mobility ratio, β, remains identical among the tested fluids, and in turn the observed variation in iDEP focusing and trapping can be attributed to solely the influence of fluid rheology via $G_D(Wi,n)G_{EK}(Wi,n)$. The inertial effect on particle motion is negligible as the calculated particle Reynolds number is much less than 1 in all cases. The estimated values of Wi based on the particle velocity inside the constriction under 200 V DC are summarized in Table 2.1.

2.4 Results and discussion

2.4.1 Newtonian buffer solution

Figure 2.3 shows the snapshot images for the iDEP focusing and trapping of 10 μm particles in the buffer solution. The particles are focused into a tight stream along the channel centerline. Moreover, the particle stream width gets narrower as the imposed DC voltage increases from 100 V to 300 V, consistent with the increasing particle velocity ratio, U_{DEP_n}/U_{EK}, in Eq. (2.7). However, when the DC voltage is partially replaced with AC voltage while their total RMS magnitude is fixed, we do not see a continuously enhanced iDEP focusing. This is because U_{DEP_n}/U_{EK} scales with the effective electric field, $(1+r^2)E_{DC}$, which is 250 V/cm for 200 V DC/100 V AC and 300 V/cm for 150 V DC/150 V AC, respectively. In other words, the iDEP focusing effect in these two DC-biased AC cases should be weaker than and equal to that under 300 V DC voltage, respectively. This analysis is validated by the experimental images in Fig. 2.3 We further carried out a two-dimensional simulation in COMSOL® to track particle trajectories

(details are referred to ref. [14]), which predicts the observed particle focusing and trapping (under 100 V DC/200 V AC) behaviors with a good agreement.

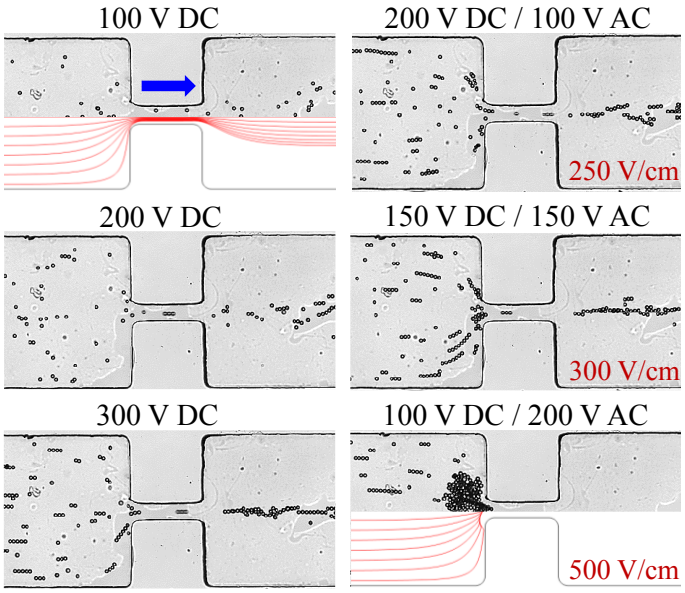

Figure 2.3 Snapshot images for the iDEP focusing and trapping of 10 μm particles in the Newtonian buffer solution through the constricted microchannel. The lower halves of the top-left and bottom-right images show the numerically predicted particle trajectories. The values of the effective electric field, $(1 + r^2)E_{DC}$, are highlighted on the images for the DC-biased AC cases. The block arrow indicates the direction of particle motion.

2.4.2 Viscoelastic PEO solution

Figure 2.4 shows the snapshot images for the electrokinetic motion of 10 μm particles in 1000 ppm PEO solution. As predicted by the particle velocity ratio, U_{DEP_n}/U_{EK}, the observed iDEP focusing in the PEO solution increases with the effective electric field, $(1 + r^2)E_{DC}$. It is, however, slightly weaker than that in the buffer solution and a complete iDEP trapping of particles is achieved under 90 V DC/210 V AC with an effective electric field of 580 V/cm (vs. 500 V/cm in the buffer solution). A quantitative comparison of the particle focusing effect between these two solutions will be presented in **Section 2.4.5** (see Fig. 2.7). Like that in the

buffer solution [52], the electroosmotic flow of the PEO solution in Fig. 2.4 exhibits a similar pattern to the electric field lines in Fig. 2.1B. We did not observe similar particle oscillation [58] or defocusing [59] in our recent works with the same particles in the same microchannel. This may be attributed to the 4 MDa PEO solution that is more viscoelastic and more shear thinning than the current 2 MDa solution. We will further explore this aspect in future work with PEO solutions that have the same concentration but varying molecular weights.

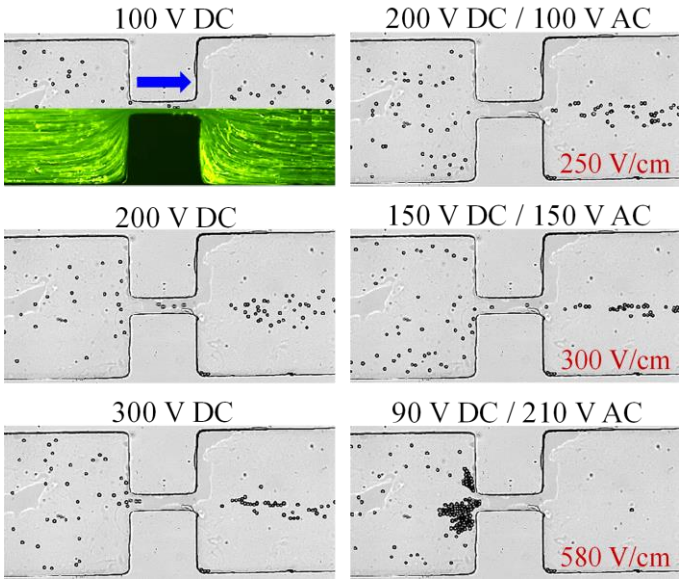

Figure 2.4 Snapshot images for the iDEP focusing and trapping of 10 μm particles in 1000 ppm PEO solution through the constricted microchannel. The lower half of the top-left image shows the experimentally obtained electroosmotic flow pattern with 0.5 μm fluorescent particles. The values of the effective electric field, $(1 + r^2)E_{DC}$, are highlighted on the images for the DC-biased AC cases. The block arrow indicates the direction of 10 μm particle motion.

The PEO solution is mildly viscoelastic ($0.1 < Wi = 0.2 < 1$) and weakly shear thinning ($n = 0.85$) with a viscosity 2.34 times the buffer solution (see Table 2.1). As the electrokinetic particle mobility is 60% of that in the buffer solution, we estimate the correction factor for electrokinetic motion, $G_{EK}(Wi, n) = 1.4$. This latter value seems reasonable considering that

fluid elasticity has no significant impact on the electroosmotic fluid velocity [31] while decreasing the opposing electrophoretic particle velocity [42]. Thus, the similar iDEP focusing and trapping for particles in the PEO and buffer solutions can be attributed to the correction factor for the drag coefficient, say $G_D(Wi, n) = 0.8$, in the PEO solution such that $G_D(Wi, n)G_{EK}(Wi, n)$ becomes slighter large than 1. This is reasonable as fluid elasticity has been reported to reduce the drag coefficient below the Newtonian fluid value [62]. An accurate understanding of the observed particle behavior calls for a numerical model that employs an appropriate constitutive equation to consider the fluid rheological effect.

2.4.3 Shear thinning XG solution

Figure 2.5 shows the stacked images for the electrokinetic motion of 10 μm particles in 1000 ppm XG solution, which is against the electric field direction yielding the only negative electrokinetic mobility in Table 2.1. Some of the particles are observed to circulate at the salient corners of the expansion walls under 100 V DC, and the size of the circulations extends both inward and downward as the DC voltage increases. Meanwhile, the rest of the particles simply travel through the constriction exhibiting no apparent focusing even under 50 V DC/250 V AC (the effective electric field is 1300 V/cm). The XG solution's inability to achieve iDEP focusing seems to be associated with the fluid circulations formed downstream in the constriction, which, as illustrated by the electroosmotic flow pattern in Fig. 2.5, is consistent with our earlier observation [52]. These fluid circulations tend to draw the particles away from their initial path after exiting the constriction, leading to a wider particle stream width because of their own size growth. Partial trapping of the particles is observed at the entrance of the constriction under 50 V DC/250 V AC. The effective electric field for a complete iDEP trapping in the XG solution

should therefore be much greater than the threshold value, 500 V/cm, in the buffer solution (see Fig. 2.3).

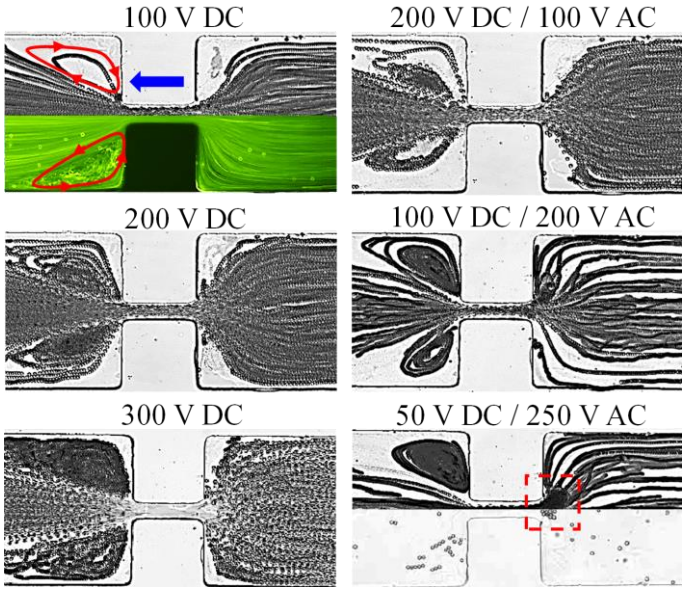

Figure 2.5 Stacked images for the electrokinetic motion of 10 μm particles in 1000 ppm XG solution through the constricted microchannel. The lower half of the top-left image shows the experimentally obtained electroosmotic flow pattern with 0.5 μm fluorescent particles, where the arrowed loops highlight the direction of circulations. The dashed-line box on the bottom-right image highlights the onset of partial iDEP trapping of particles, illustrated by the stacked and snapshot images in the upper and lower halves, respectively. The block arrow indicates the direction of particle motion.

As the electrokinetic particle mobility in the XG solution has a similar magnitude to that in the buffer solution while the former is far more viscous (9.4 times the latter, see Table 2.1), we expect the correction factor for electrokinetic motion , $G_{EK}(Wi, n) = 9$, for the strongly shear thinning XG solution ($n = 0.36$). This value seems possible because the fluid shear thinning effect has been reported to increase both the electroosmotic [31] and electrophoretic [39] velocities. The fluid shear thinning effect has also been reported to increase the drag coefficient above the Newtonian fluid value, i.e., $G_D(Wi, n) > 1$ [63]. Therefore, we obtain

$G_D(Wi,n)G_{EK}(Wi,n) \gg 1$, which, according to Eq. (2.8), should indicate a strongly elevated threshold electric field for iDEP trapping of particles. This analysis is consistent with our experiment in Fig. 2.5 as noted above.

2.4.4 Viscoelastic and shear thinning PAA solution

Figure 2.6 shows the snapshot images for the electrokinetic motion of 10 μm particles in 100 ppm PAA solution, where the strongest iDEP focusing and trapping are observed among the tested fluids. Particles achieve a good focusing under 200 V DC and a complete trapping under 300 V DC (note a partial trapping occurs under 250 V DC). The electroosmotic flow streamlines still resemble the electric field lines like in the PEO solution. They are, however, different from our recent observation, where a central fluid jet is formed downstream in a more viscoelastic and more shear thinning 200 ppm PAA solution [52]. As viewed from Table 2.1, 100 ppm PAA solution is strongly viscoelastic ($Wi \gg 1$) and shear thinning ($n = 0.54$) with a viscosity about 2.2 times the buffer solution. The electrokinetic particle mobility in this solution is 90% of that in the buffer. The estimated correction factor for electrokinetic motion is $G_{EK}(Wi,n) = 2$, which can be attributed to the fluid elasticity effect like in the PEO solution. Hence, the strongest iDEP focusing and trapping of particles in the PAA solution results from the correction factor for the drag coefficient, $G_D(Wi,n) < 0.5$, such that $G_D(Wi,n)G_{EK}(Wi,n) < 1$. This may be caused by the strong fluid elasticity and perhaps the second normal stress difference as well [64], necessitating a numerical model with an appropriate constitutive equation for the full rheological effects.

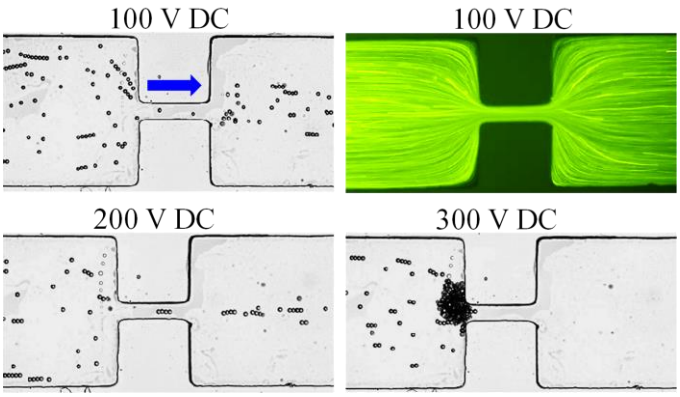

Figure 2.6 Snapshot images for the iDEP focusing and trapping of 10 μm particles in 100 ppm PAA solution through the constricted microchannel. The top-right image shows the experimentally obtained electroosmotic flow pattern with 0.5 μm fluorescent particles. The block arrow indicates the direction of particle motion.

2.4.5 Comparison among the tested fluids

Figure 2.7 compares the experimentally measured widths of the focused 10 μm particle streams (normalized by the channel width) downstream in the buffer, PEO and PAA solutions. The XG solution is excluded from the figure because no apparent iDEP focusing is observed. Note the zero-stream width indicates a complete iDEP trapping of particles. As predicted from Eq. (2.7), particles in the three fluids experience an enhanced iDEP focusing effect (i.e., smaller particle stream width) with the increase of the effective electric field, $(1 + r^2)E_{DC}$. Moreover, the three curves exhibit a similar shape, validating the first and second order dependences on electric field for the electrokinetic and dielectrophoretic particle velocities, respectively, in viscoelastic solutions. Our experiment tells that fluid shear thinning causes strong disturbances to the electroosmotic flow and in turn suppresses the iDEP focusing effect. It also reduces the iDEP trapping of particles because of the decreased dielectrophoretic velocity and increased electrokinetic velocity. On the contrary, fluid elasticity stabilizes the electroosmotic flow and enhances the iDEP focusing/trapping because of the increased electrokinetic and

dielectrophoretic velocities. The combination of fluid shear thinning and elasticity may cause an enhancement or reduction depending on which effect is stronger.

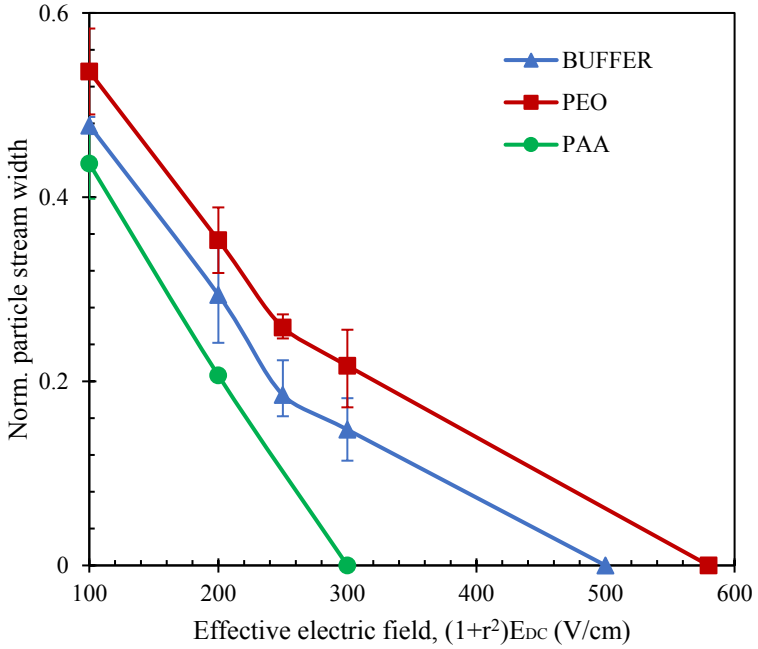

Figure 2.7 Comparison of the average normalized particle stream width, n=3, (normalized by the channel width) for the iDEP focusing of 10 μm particles in the tested fluids. Note the zero-stream width indicates a complete iDEP trapping.

2.5 Concluding remarks

We have experimentally studied in the same constricted microchannel the electrokinetic motion of polystyrene particles in three types of non-Newtonian fluids with distinct rheological properties. We have also revised the theory for iDEP focusing and trapping of particles in Newtonian fluids by introducing correction factors to account for the fluid rheological effects on the electrokinetic and dielectrophoretic motions, respectively. It is found that the iDEP focusing and trapping effects in the mildly viscoelastic PEO solution are slightly weaker than in the Newtonian buffer solution. They are, however, significantly improved in the PAA solution that is

strongly viscoelastic and shear thinning. The measured particle stream widths in the buffer, PEO and PAA solutions exhibit a similar relation with respect to the effective electric field, consistent with our theoretical analysis. In contrast, no apparent iDEP focusing of particles is achieved in the strongly shear thinning XG solution though the iDEP trapping can take place under a much larger effective electric field than the other fluids. We have attempted to explain the observed particle focusing and trapping behaviors using the introduced correction factors. It is expected this experimental work will stimulate more numerical studies in the future.

2.6 References

[1] Tang, W., Jiang, D., Li, Z., Zhu, L., Shi, J., Yang, J., Xiang, N., *Electrophoresis* 2019, *40*, 930-954.

[2] Zhang, S., Wang, Y., Onck, P., den Toonder, J., *Microfluid. Nanofluid.* 2020, *24*, 24.

[3] Herrmann, N., Neubauer, P., Birkholz, M., *Biomicrofluidics* 2019, *13*, 061501.

[4] Zhao, Q., Yuan, D., Zhang, J., Li, W., *Micromachines* 2020, *11*, 461.

[5] Tang, W., Zhu, S., Jiang, D., Zhu, L., Yang, J., Xiang, N., *Lab Chip* 2020, *20*, 3485-3502.

[6] Lu, X., Liu, C., Hu, G., Xuan, X., *J. Colloid Interface Sci.* 2017, *500*, 182–201.

[7] Tian, F., Feng, Q., Chen, Q., Liu, C., Li, T., Sun, J., *Microfluid. Nanofluid.* 2019, *23*, 68.

[8] Zhou, J., Papautsky, I., *Microsys. Nanoeng.* 2020, *6*, 113.

[9] Connacher, W., Zhang, N., Huang, A., Mei, J., Zhang, S., Gopesh, T., Friend, J., *Lab Chip* 2018, *18*, 1952-1996.

[10] Zhang, P., Bachman, H., Ozcelik, A., Huang, T. J., *Annu. Rev. Anal. Chem.* 2020, *13*, 17-43.

[11] Xuan, X., *Micromachines* 2019, *10*, 744.

[12] Munaz, A., Shiddiky, M. J. A., Nguyen, N. T., *Biomicrofluid.* 2018, *12*, 031501.

[13] Yang, H., Gijs, M. A. M., *Chem. Soc. Rev.* 2018, *47*, 1391-1458.

[14] Zhu, J., Xuan, X., *Electrophoresis* 2009, *30*, 2668-2675.

[15] Braff, W. A., Pignier, A., Buie, C. R., *Lab Chip* 2012, *12*, 1327-1331.

[16] Barrett, L. M., Skulan, A. J., Singh, A. K., Cummings, E. B., Fiechtner, G. J., *Anal. Chem.* 2005, *77*, 6798-6804.

[17] Nakano, A., Camacho-Alanis, F., Ros, A., *Analyst* 2015, *140*, 860-868.

[18] Kale, A., Lu, X., Patel, S., Xuan, X., *J. Micromech. Microeng.* 2014, *24*, 075007.

[19] Lewpiriyawong, N., Yang, C., Lam, Y.C., *Microfluid. Nanofluid.* 2012, *12*, 723-733.

[20] Saucedo-Espinosa, M. A., Lapizco-Encinas, B. H., *Electrophoresis* 2015, *36*, 1086-1097.

[21] Pudasaini, S., Perera, A. T. K., Das, D., Ng, S H., Yang, C., *Electrophoresis* 2019, *40*, 2522-2529.

[22] Pysher, M. D., Hayes, M. A., *Anal. Chem.* 2007, *79*, 4552-4557.

[23] Gallo-Villanueva, R. C., Pérez-González, V. H., Davalos, R. V., Lapizco-Encinas, B. H., *Electrophoresis* 2011, 32, 2456-2465.

[24] Hill, N., Lapizco-Encinas, B. H., *Anal. Bioanal. Chem.* 2020, *412*, 3891–3902.

[25] Lapizco-Encinas, B. H., *Electrophoresis* 2019, *40*, 358-375.

[26] Xuan, X., *Electrophoresis* 2019, *40*, 2484-2513.

[27] Lapizco-Encinas, B. H., *Curr. Opinion Chem. Eng.* 2020, *29*, 9-16.

[28] Bird, R. B., Armstrong, R. C., Hassager, O., *Dynamics of Polymeric Liquids*, Willey, vol.1, 1977.

[29] M. Brust, C. Schaefer, R. Doerr, L. Pan, M. Garcia, P. E. Arratia, and C. Wagner, *Phys. Rev. Lett.* 2013, *110*, 078305.

[30] D'Avino, G., Maffettone, P. L., *J. Non-Newton. Fluid Mech.* 2015, *215*, 80-104.

[31] Zhao, C., Yang, C., *Adv. Colloid. Interf. Sci.* 2013, *201–202*, 94–108.

[32] Zhao, C., Yang, C., *Biomicrofluidics* 2011, *5*, 014110.

[33] Afonso, A. M., Pinho, F.T., Alves, M. A., *J. Non-Newtonian Fluid Mech.* 2012, *179-180*, 55-68.

[34] Zhao, C., Yang, C., *Electrophoresis* 2013, *34*, 662-667.

[35] Ferrás, L. L., Afonso, A. M., Alves, M. A., Nóbrega, J. M., Pinho, F. T., *Phys. Fluids* 2016, *28*, 093102.

[36] Mei, L., Zhang, H., Meng, H., Qian, S., *Micromachines* 2018, *9*, 155.

[37] Mei, L., Qian, S., *Micromachines* 2019, *10*, 747.

[38] Lee, E., Chen, C. T., Hsu, J. P., *J. Colloid Interface Sci.* 2005, *285*, 857–864.

[39] Yeh, L. H., Hsu, J. P., *Microfluid. Nanofluid.* 2009, *7*, 383–392.

[40] Khair, A. S., Posluszny, D. E., Walker, L. M., *Phys. Rev. E* 2012, *85*, 016320.

[41] Zhou, T., Deng, Y., Zhao, H., Zhang, X., Shi, L., Joo, S. W., *J. Fluids Eng.* 2018, *140*, 091302.

[42] Li, G., Koch, D. L., *J. Fluid Mech.* 2020, *884*, A9.

[43] Chang, F. M., Tsao, H. K., *Appl. Phys Lett.* 2007, *90*, 194105.

[44] Mukherjee, S., Das, S. S., Dhar, J., Chakraborty, S., DasGupta, S., *Langmuir* 2017, 33, 12046–12055.

[45] Huang, Y., Chen, J., Wong, T. N., Liow, J.-L., *Soft Matt.* 2016, *12*, 6206-6213.

[46] Moschopoulos, P., Dimakopoulos, Y., Tsamopoulos, J., *J. Colloid Interf. Sci.* 2020, *563*, 381–393.

[47] Bryce, R. M., Freeman, M. R., *Phys. Rev. E* 2010, *81*, 036328.

[48] Sadek, S. H., Pinho, F. T., Alves, M. A., *J. Non-Newton. Fluid Mech.* 2020, *283*, 104293.

[49] Pimenta, F., Alves, M. A., *J. Non-Newton. Fluid Mech.* 2018, *259*, 61-77.

[50] Afonso, A. M., Pinho, F.T., Alves, M. A., *J. Non-Newtonian Fluid Mech.* 2012, *179-180*, 55-68.

[51] Bezerra, W. D. S., Castelo, A., Afonso, A. M., *Micromachines* 2019, *10*, 796.

[52] Ko, C. H., Li, D., Malekanfard, A., Wang, Y. N., Fu, L. M. and Xuan, X., *Electrophoresis* 2019, *40*, 1387-1394.

[53] Malekanfard, A., Ko, C. H., Li, D., Bulloch, L, Baldwin, A., Wang, Y. N., Fu, L. M., Xuan, X., *Phys. Fluids* 2019, *31*, 022002.

[54] Li, D., Xuan, X., *Phys. Rev. Fluid.* 2018, *3*, 074202.

[55] Choudhary, A., Li, D., Renganathan, T., Xuan, X., Pushpavanam, S., *J. Fluid Mech.* 2020, *898*, A20.

[56] Khair, A. S., Kabarowski, J. K., *Phys. Rev. Fluids* 2020, *5*, 033702.

[57] Zhang, A., Murch, W. L., Einarsson, J., Shaqfeh, E. S. G., *J. Non-Newton. Fluid Mech.* 2020, *280*, 104279.

[58] Lu, X., Patel s., Zhang, M., Woo, S., Qian, S., Ogale, A. and Xuan, X., *Biomicrofluidics* 2014, *8*, 021802.

[59] Lu, X., DuBose, J., Woo, S., Qian, S., and Xuan, X., *Biomicrofluidics* 2015, *9*, 014108.

[60] Acharya, A., Mashelkar, R. A., Ulbrecht, J., *Rheol. Acta* 1976, *15*, 454-470.

[61] Alizadeh, A., Hsu, W.-L., Wang, M., Daiguji, H., *Electrophoresis* 2021, *42*, in press. https://doi.org/10.1002/elps.202000313

[62] Chhabra, R. P., Uhlherr, P. H. T., Boger, D. V., *J. Non-Newton. Fluid Mech.* 1980, *6*, 187-199.

[63] Siili, D., Coutanceau, M., *J. Non-Newton. Fluid Mech.* 1977, *2*, 1-21.

[64] Villone, M. M., D'Avino, G., Hulsen, M. A., Greco, F., Maffettone, P. L., *J. Non-Newton. Fluid Mech.* 2013, *195*, 1–8.

[65] Rodd, L. E., Scott, T. P., Boger, D. V., Cooper-White, J. J., McKinley, G. H., J. *Non-Newton. Fluid Mech*. 2005, 129, 1–22.

[66] Lindner, A., Bonn, D., Meunier, J.*, Phys. Fluids* 2000, 12, 256–261.

[67] Poole, R. J., Escudier, M. P., *J. Non-Newton. Fluid Mech.* 2004, *117*, 25–46.

[68] Kulicke, W.-M., Kniewske, R., Klei, J., *Prog. Polymer Sci.* 1982, *8*, 373-468.

[69] Ermolina, I., Morgan, H. *J. Colloid Interface. Sci.* 2005, *285*, 419–428.

CHAPTER 3

FLUID RHEOLOGICAL EFFECTS ON STREAMING DIELECTROPHORESIS IN A POST-ARRAY MICROCHANNEL

3.1 Background on DEP and electroosmosis in Post-Array Micro-channel

Today, microfluidic manipulation of particles and cells has garnered significant development due its impact in solving challenges in the fields of analytical chemistry, bioanalysis, cell biology and clinical applications [1-3]. Its relevance has compelled research into the use of various force fields (e.g., externally imposed acoustic [4,5], magnetic [6,7], optical [8], and electric [9]) for its implementation. Insulator-based Dielectrophoresis (iDEP) has been widely used in recent times to achieve particle manipulation in microfluidic devices mostly in Newtonian fluids. It involves the use of insulating structures to create electric field gradients for continuous flow focusing [10,11], trapping [12,13], patterning [14], concentration [15,16], poration [17] and separation [18-20] of particles. However, many biological (e.g., blood, saliva DNA solutions, etc.) and chemical (e.g., polymer and colloidal solutions) fluids demonstrate non-Newtonian behaviors making it crucial to understand the effects of fluid rheological properties on iDEP focusing and trapping of particles.

Our group, recognizing the importance of investigations in non-Newtonian fluids, has recently performed an experimental study on the sole and combined effects of fluid elasticity and shear

thinning on electroosmotic flow and particle manipulation (focusing and trapping) due to iDEP in a constricted microchannel [21,22]. Fluid shear-thinning was observed to cause flow circulations in the xanthan gum which increase in size with applied DC electric field and temporarily trap particles (without the influence of iDEP). Meanwhile, fluid elasticity is observed to stabilize flow in Polyvinylpyrrolidone (PVP) and PEO. iDEP effects for particle focusing and trapping are seen to be diminished in the shear-thinning weakly elastic XG solution and strongly enhanced in the shear-thinning viscoelastic PAA solution. Weakly elastic, mildly viscoelastic PEO exhibit slightly weaker iDEP effects in relation to Newtonian solution. We employed the use of correction factors to account for the effects of fluid rheology on particle electrokinetic mobility and drag which were supported by the experimentally obtained results.

Complex geometries can dramatically alter the flow behavior of polymers based on their structure. Presently, knowledge on such flow behaviors in porous media are often used with polymer solutions for various applications such as oil recovery and groundwater remediation [23-25] where polymer solutions are injected through porous medium to displace trapped non-aqueous fluids from pore spaces to be retrieved downstream. The post-array structure is a type of porous medium reported to cause elastic build up which affects fluid flow and particle motion in pressure driven flows [26]. This is due to the tortuous nature of the pore spaces which the fluids must navigate causing the elongation and contraction of polymer structures. We hypothesize a similar effect even with the reduced velocities and shear rates associated with electric driven flows such that non-Newtonian fluids under this condition should behave differently in comparison to observations in the single constriction channel from our previous work [21,22]. We expect that the changes in flow behavior of the polymer solutions should influence the manipulation of particles by iDEP forces.

3.2 Experiment

3.2.1 Materials

The microfluidic device for this experiment is fabricated from polydimethylsiloxane (PDMS) using the soft lithography technique. The detailed methodology used is reported in section 2.2.2. The device contains a 1 cm-long straight channel with main width and depth of 800um and 50um respectively. A 3 x 6 array of circular posts with diameters of 200um are positioned in the middle of the channel. These posts are equally spaced at 50um between post circumferences. A schematic representation on the microchannel used is shown in Fig. 3.1. Polystyrene particles of 10um diameter (Sigma-Aldrich) were used to demonstrate the iDEP focusing and trapping while florescent polystyrene spheres of 1um diameters (Bangs Laboratories) were used as tracers to visualize the flow patterns. These were re-suspended into three types of non-Newtonian fluids that were each prepared in 1mM phosphate buffer: (1) viscoelastic 1000 ppm PEO solution ($M_w = 2$ MDa, Sigma-Aldrich); (2) shear-thinning 1000 ppm xanthan gum (XG) solution (Tokyo Chemical Industry); (3) viscoelastic and shear-thinning 100 ppm PAA solution ($M_w =$ 18 MDa, Polysciences). Newtonian solutions were prepared by re-suspending these particles in pure buffer and served as the controls. Tween 20 (0.5% v/v, Fisher Scientific) was added to each prepared particle suspension for suppressing the particle-wall adhesions. The important rheological properties are summarized in Table 2.1.

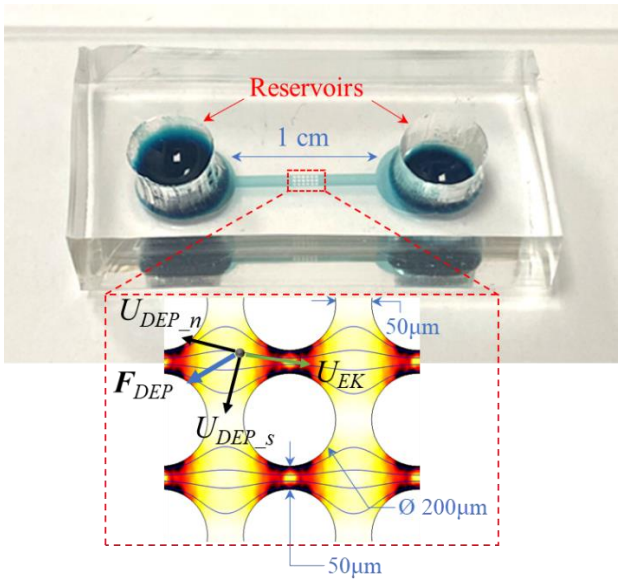

Figure 3.1 Picture of the fabricated microfluidic chip where the post-array microchannel and reservoirs are filled with green food dye for clarity. The inset is a representation of the 3x6 array of circular posts. It illustrates the iDEP focusing and trapping of particles in the constriction regions of the microchannel, where the electric field gradient-induced dielectrophoretic force, $\boldsymbol{F}_{DEP}$, drives both a cross-stream particle motion, U_{DEP_n}, for focusing, and a streamwise particle motion, U_{DEP_s}, for trapping because it opposes the electrokinetic particle motion, U_{EK}. The background shows the electric field lines and the contour for the gradient of electric field squared, $\nabla \boldsymbol{E}^2$ (the darker the larger magnitude).

3.2.2 Methods

A function generator (33220A, Agilent Technologies) and a high-voltage amplifier (609E-6, Trek) supplied pure DC or DC-biased AC electric fields to drive the particle suspensions through the post-array microchannel. The electroosmotic patterns were studied by observing the fluorescent tracers as pure DC electric fields are applied up to 500 V. For observations for dielectrophoretic particle focusing and trapping, DC voltages of up to 500 V were first applied. If no particle focusing or trapping was achieved, DC-biased AC voltages with a total root-mean-square (RMS) magnitude of 500V were then used for enhanced iDEP effects. The average electric field through the microchannel was thus limited to a maximum of 500V/cm across the 1 cm long microchannel. Electroosmotic flow patterns and particle motion within the post-array

region were recorded using a microscope (Nikon Eclipse TE2000U, Nikon Instruments) equipped with a CCD camera (Nikon DS-Qi1Mc). Observed images were within a considerable period after electric field was applied when steady state was achieved and were processed using the Nikon Imaging Software (NIS-Elements AR 2.30).

3.3 Results and discussion

3.3.1 Newtonian buffer solution

Figure 2 show super-imposed microscopic images for the iDEP focusing and trapping of 10um particle in the Newtonian buffer solution. A total of four particle streams are formed between adjacent posts as well as between post and walls. iDEP focusing effect generally increases with increasing effective electric field applied which is consistent with our previous results in constriction channels as well as theory. It is also observed that particle stream width decreases as particles travel streamwise through the rows of posts. This can be associated with the continuous repulsion of electrokinetic velocities of particles as they travel through post by constant dielectrophoretic forces which push the particles towards the centerline of the streams. Particles are not seen to cross between streams in Newtonian fluids. The electroosmotic flow pattern corroborates this as it is observed that florescent 0.5um bangs particles do not travel laterally between posts (zoomed in images at lower right corner). IDEP particle trapping is not realized within the pure DC electric field limits hence the need to apply DC-biased AC electric field. Trapping is realized at 100 V DC/400 V AC which has an effective electric field of 1700 V/cm. The trapping phenomenon associated with iDEP for post array channels manifest such that the particles fall on the post in their direction of motion when electrokinetic velocities are completely overwhelmed by dielectrophoretic velocities as observed by Saucedo-Espinosa et al

[16]. Experimental results are in good agreement with two-dimensional simulation carried out in COMSOL® to track particle trajectories.

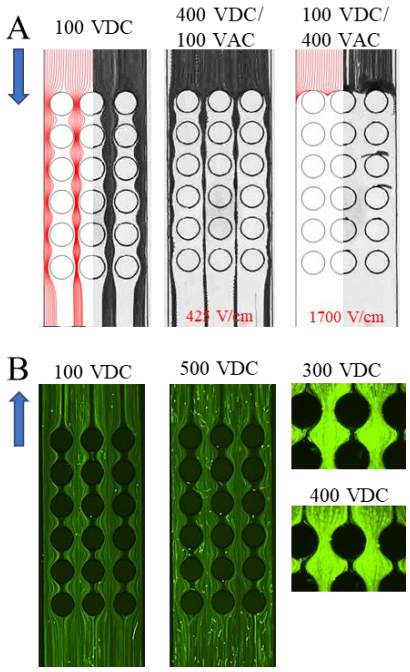

Figure 3.2 (A) Superimposed images for the iDEP focusing and trapping of 10 μm particles in the Newtonian buffer solution through the post-array microchannel. Left half images of 1st and 3rd images (counting from the left) show the numerically predicted particle trajectories. The values of the effective electric field, $(1 + r^2)E_{DC}$, are highlighted on the images for the DC-biased AC cases. (B) Shows the streak images of tracing articles under DC electric fields as a representation of the electroosmotic flow pattern of the Newtonian solution. Zoomed in images at 300VDC and 400VDC are shown on the right. Block arrows in both cases represent the direction of particles in motion.

3.3.2 Viscoelastic PEO solution

The PEO solution used has weakly sheathinning and midly viscoelastic characterisics. Fig. 3.3 shows the superimposed microscopic images for the electrokinetic particle motion of 10μm particles and the electroosmotic flow pattern. Similar trends to the Newtonian case are observed with iDEP focusing effect enhancing with increasing applied effective electric field as predicted by the velocity ratio, U_{DEP_n}/U_{EK}. It is however observed that the iDEP effect is weaker in comparison to Newtonian case. Focusing at 500V DC in the PEO solution is not as enhanced as

that in Newtonian solutions. Complete trapping occurs at 80V DC/ 420V AC which is at an effective electric field of 2285V/cm. The trapping occurrence is the same as for the Newtonian case.

Electroosmotic flow shows a similar pattern to what is observed in the Newtonian flows. We hypothesize that this similarity is because the short PEO 2M chain lengths do not generate substantial elastic stress build up as they curve with streamlines. The eddies associated with the elastic stresses are not observed within the lateral spaces between the posts such that there is no transfer of tracer particles between streams.

These similar electrokinetic and electroosmotic trends of Newtonian and PEO solutions are identical to observations made in our previous work with constriction channels where PEO solution also showed relatively weaker iDEP effect [22] and visually analogous electroosmotic flow pattern [21].

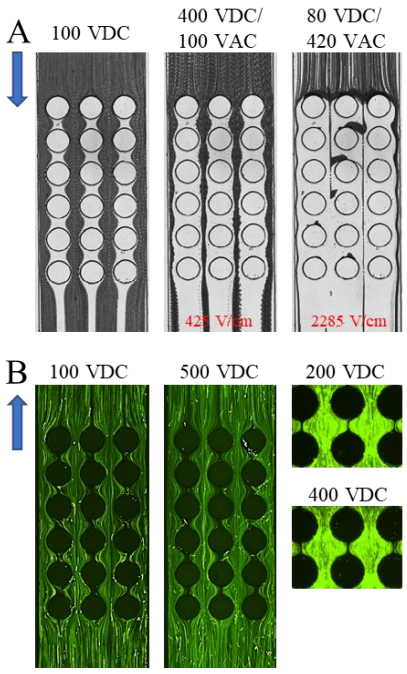

Figure 3.3 (A) Superimposed images for the iDEP focusing and trapping of 10 μm particles in the PEO solution through the post-array microchannel. The values of the effective electric field,

$(1 + r^2)E_{DC}$, are highlighted on the images for the DC-biased AC cases. (B) Shows the streak images of tracing articles under DC electric fields as a representation of the electroosmotic flow pattern of the Newtonian solution. Zoomed in images at 200VDC and 400VDC are shown on the right. Block arrows in both cases represent the direction of particles in motion.

The PEO solution is mildly viscoelastic (0.1<Wi=0.2<1) and weakly shear thinning (n=0.85) with viscosity 2.34 times the buffer solution (see Table 2.1). Similar trends with our work in constriction channels corroborate our estimation of the correction factors regarding equations (1) and (2). Based on the lower particle mobility of PEO in comparison to the Newtonian solution, we estimated an electrokinetic correction factor as $G_{EK}(Wi, n) = 1.4$. This estimation is reasonable because while fluid elasticity has insignificant impact on electroosmotic fluid velocity, it decreases the opposing electrophoretic particle velocity. The correction factor for the drag coefficient is then estimated as $G_D(Wi, n) = 0.8$, such that the product of both correction factors is slightly larger than 1. This accounts for the similar but slightly weaker iDEP focusing and trapping effect for particles in PEO in comparison to Newtonian solutions. Our estimation of the drag correction factor is validated by the reports claiming fluid elasticity reduce the drag coefficient below the Newtonian fluid value [28].

3.3.3 Shear thinning XG solution.

Fig. 3.4 shows super-imposed images for the electrokinetic particle motions and electroosmotic flow patterns for electric fields applied. Electrokinetic particle motion is from the cathode to the anode which is contrary to observations in other fluids for this study. This phenomenon is observed in our previous work in the constriction channel. iDEP particle focusing is not enhanced with increase effective field applied. Particle circulations are observed within the

lateral spaces between posts at low DC electric fields as shown in dashed circles on left image of Fig. 3.4A. This is consistent with observations made in the electrokinetic and electroosmotic flow patterns for constriction channel and has been reported to be related to fluid shear-thinning effects [22,23]. These circulations can be associated with eddies formed as a result of elastic stresses generated. The circulations prevent the enhancement of iDEP focusing in XG solution as particles are diverted off their trajectory after exiting the constrictions. It is also observed in the electroosmotic flow pattern that 0.5um fluorescent particles travel across streams in the XG solution. For the electrokinetic experiment, this occurs for 10um Sigma particles at DC electric fields of 300 V and above. This can be associated with larger circulations formed at these electric fields which are able to trap particles and transfer them into other streams due to the overlap. IDEP particle trapping is not realized for the XG solution during the experiment. An interesting phenomenon worth mentioning is the apparent flow instability at 400 V DC and above characterized by the formation of gels which appear to prevent the motion of tracer particles highlighted by dashed boxes in Fig. 3.4. We hypothesize that, despite the weakly elastic nature of XG, its long polymer structure generates significant elastic stress build up to create instabilities in flow for the electroosmotic velocities at these electric fields. This instability occurs at about 5-8 seconds after the 400V DC electric field is applied signifying some sort of buildup of the afore discussed stresses. This is corroborated by the electroosmotic flow pattern at that electric field where a similar incident occurs at 500VDC. This occurrence cannot be associated with enhanced iDEP effect as the manifestation varies greatly from observations in the Newtonian and PEO cases. Also, particle circulations are noticed within longitudinal spaces between post while particles within streams generally travel toward the anode at 100VDC/400VAC at low electrokinetic velocities in comparison to the pure 100V DC case

without any observed iDEP effect. This is indicative of AC electric fields possibly influencing particle mobility in the XG solution.

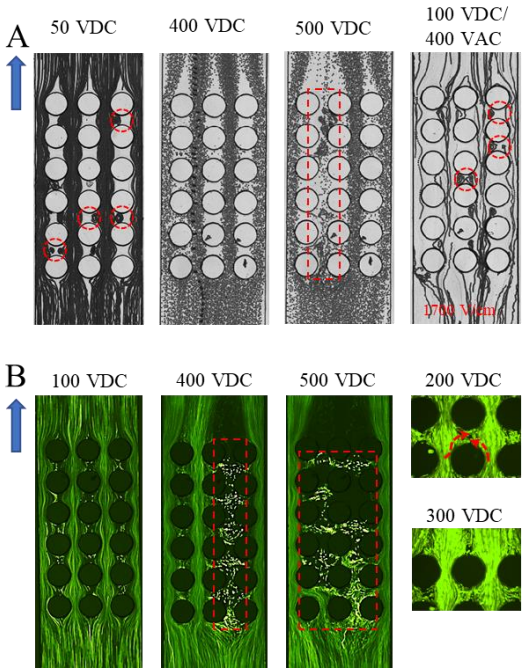

Figure 3.4 (A) Superimposed images for the iDEP focusing and trapping of 10 μm particles in the 1000ppm XG solution through the post-array microchannel. The values of the effective electric field, $(1 + r^2)E_{DC}$, are highlighted on the lower part of image for the DC-biased AC case. (B) Shows the streak images of tracing particles under DC electric fields as a representation of the electroosmotic flow pattern of the Newtonian solution. Zoomed in images at 200VDC and 300VDC are shown on the right. Block arrows in both cases represent the direction of particles in motion. Dashed circles highlight the particle circulations while dash boxes indicate gels formations. Dashed arrows indicate the transfer of tracer particles between streams through lateral spaces between spaces.

This suppressed iDEP effect in XG solution is observed in our work with constriction channel and further corroborates our earlier estimated electrokinetic and drag correction factors of $G_{EK}(Wi, n) = 9$ and $G_D(Wi, n) > 1$ respectively. Both estimates are reasonable based on reports that shear thinning increase both electroosmotic [29] and electrophoretic [30] velocities which influence the electrokinetic correction factor. It also increases drag coefficient above the Newtonian fluid value such that $G_D(Wi, n) > 1$[31]. The product of the correction factors,

$G_D(Wi,n)G_{EK}(Wi,n) \gg 1$, which indicate strongly elevated threshold electric field for iDEP trapping of particles based on Eq. 2.8.

3.3.4 Viscoelastic and shear thinning PAA solution

Fig. 3.5 shows the snapshot images of electrokinetic particle motion for PAA solution. 100ppm PAA solution has shear thinning ($Wi \gg 1$) and viscoelastic ($n = 0.54$) characteristics. iDEP particle focusing was observed to improve as DC electric field is increased up to 100VDC. Beyond this DC electric field, 10um Sigma particles in the PAA solution are seen to coagulate within and upstream of the post as an indication of instability. This also occurs in the DC-biased AC electric fields applied for DC voltages of 200VDC and above regardless of the AC electric field applied. Thus, we deduce this occurrence is dependent on the DC electric field applied but independent of iDEP effects. An analogous observation is made regarding the electroosmotic flow patterns in PAA solutions where the florescent particles are seen to form blobs as they move along the streams at 200VDC. Also, florescent particles are observed to travel across streams through lateral spaces between posts indicating the presence of eddies associated with elastic stresses. Beyond 300VDC, gels are formed at rates depending on the electric field applied in both electroosmotic and electrokinetic observations and prevent the iDEP focusing of particles. We hypothesize that PAA 18MDa presents substantial polymer chain lengths that generate normal elastic stress as described in section 3. The instability in PAA realized before the influence of the posts can be associated with some kind of predictive effect such that polymer chain behaviors within the post array influence strains further upstream. IDEP effects are noticed as particle focusing is enhanced from 150VDC/350VAC to 100VDC/400VAC. Particle motion

at these electric fields resemble that in PEO and Newtonian case. Trapping occurs at 50VDC/450VAC with an effective electric field of 4100V/cm.

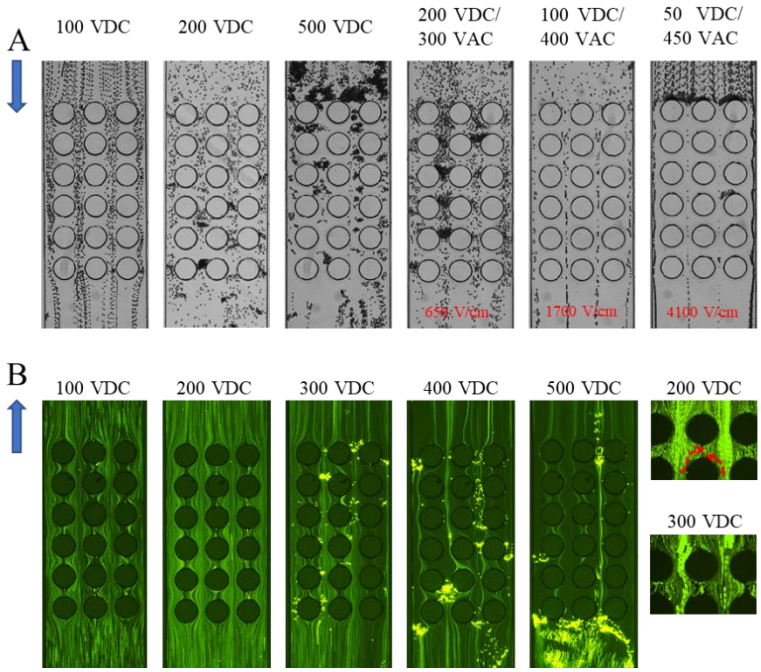

Figure 3.5 (A) Snapshot images for the iDEP focusing and trapping of 10 μm particles in the 100ppm PAA solution through the post-array microchannel. The values of the effective electric field, $(1 + r^2)E_{DC}$, are highlighted on the lower part of images for the DC-biased AC cases. (B) Shows the streak images of tracing particles under DC electric fields as a representation of the electroosmotic flow pattern of the Newtonian solution. Zoomed in images at 200VDC and 300VDC are shown on the right. Block arrows in both cases represent the direction of particles in motion. Dashed arrows indicate the transfer of tracer particles between streams through lateral spaces between spaces.

The electrokinetic particle mobility of PAA has a similar magnitude to that in the Newtonian solution but is 2.24 times more viscous that the latter. Thus, we estimate an electrokinetic correction factor of $G_{EK}(Wi, n) = 4$, for the shear thinning ($n = 0.54$), viscoelastic ($1 < Wi = 10$) PAA solution. This is a reasonable estimation as shear thinning effect has been reported to increase both the electroosmotic [29] and electrophoretic [30] velocities while viscoelasticity decreases the electrophoretic particle velocity [32]. The resulting net effect is an increase in

electroosmotic velocity which essentially improves electrokinetic velocities. Fluid shear thinning has also been reported to increase drag coefficient [31] while viscoelasticity has contradictory effects. The PAA solution exhibits more viscoelastic than shear thinning effects thus an estimated drag correction factor of $G_D(Wi, n) = 0.6$ depicts the overpowering effects of viscoelasticity. Therefore, we obtain $G_D(Wi, n)G_{EK}(Wi, n) = 2.4$, which indicates an elevated threshold electric field for iDEP trapping of particles which is observed experimentally.

3.4 Concluding remarks

We have experimentally studied the electroosmotic flow patterns ad electrokinetic motion of 0.5 um Bangs florescent particles and 10um Sigma polystyrene particles in three types of non-Newtonian fluids with distinct rheological properties in the same post-array microchannel. We utilize the theory we revised for iDEP focusing and trapping of particles in non-Newtonian fluids from our previous work. Generally, this theory has been consistent for our work with constriction channels and with post-array channels. However, some interesting phenomena are observed for the electrokinetic motion and electroosmotic flow patterns which we hypothesize are correlations between the polymer structures and microchannel structure. We discovered that iDEP focusing and trapping effects in the mildly viscoelastic PEO solution are slightly weaker than in the Newtonian buffer solution for the post-array channel while electroosmotic flow patterns are similar between both solutions for the post-array channels. Flow instabilities are observed for the shear-thinning and weakly elastic XG solution when DC electric field exceed certain limits. The occurrence is consistent with observations in the electrokinetic motion of particles in XG solution. No apparent iDEP focusing and trapping of particle is observed which is consistent with the constriction microchannel case. Shear-thinning and viscoelastic PAA solutions also

exhibits unstable behavior at certain DC electric fields for both electroosmotic flow patterns and electrokinetic motion observations. However, iDEP focusing and trapping effects significantly weaker than the Newtonian case which is contrary to observations in the constriction microchannel.

3.5 References

[1] Zhang, S., Wang, Y., Onck, P., den Toonder, JMJ., *Microfluid. Nanofluid.* 2020, *24,* 24.

[2] Xuan, X., Zhu, J., Church, C., *Microfluid. Nanofluid.* 2010, *9,* 1–16.

[3] Cetina, B., Özer, M. B., Solmaz, M. E., *Biochemical Engineering Journal.* 2014, *92,* 63-82.

[4] Zhou, J., Papautsky, I., *Microsys. Nanoeng.* 2020, *6*, 113.

[5] Connacher, W., Zhang, N., Huang, A., Mei, J., Zhang, S., Gopesh, T., Friend, J., *Lab Chip* 2018, *18*, 1952-1996.

[6] Zhang, P., Bachman, H., Ozcelik, A., Huang, T. J., *Annu. Rev. Anal. Chem.* 2020, *13*, 17-43.

[7] Xuan, X., *Micromachines* 2019, *10*, 744.

[8] Munaz, A., Shiddiky, M. J. A., Nguyen, N. T., *Biomicrofluid.* 2018, *12*, 031501.

[9] Xuan, X., *Electrophoresis* 2019, *40,* 2484–2513.

[10] Zhu, J., Xuan, X., *Electrophoresis* 2009, *30*, 2668-2675.

[11] Braff, W. A., Pignier, A., Buie, C. R., *Lab Chip* 2012, *12*, 1327-1331.

[12] Barrett, L. M., Skulan, A. J., Singh, A. K., Cummings, E. B., Fiechtner, G. J., *Anal. Chem.* 2005, *77*, 6798-6804.

[13] Nakano, A., Camacho-Alanis, F., Ros, A., *Analyst* 2015, *140*, 860-868.

[14] Kale, A., Lu, X., Patel, S., Xuan, X., *J. Micromech. Microeng.* 2014, *24*, 075007.

[15] Lewpiriyawong, N., Yang, C., Lam, Y.C., *Microfluid. Nanofluid.* 2012, *12*, 723-733.

[16] Saucedo-Espinosa, M. A., Lapizco-Encinas, B. H., *Electrophoresis* 2015, *36*, 1086-1097.

[17] Pudasaini, S., Perera, A. T. K., Das, D., Ng, S H., Yang, C., *Electrophoresis* 2019, *40*, 2522-2529.

[18] Pysher, M. D., Hayes, M. A., *Anal. Chem.* 2007, *79*, 4552-4557.

[19] Gallo-Villanueva, R. C., Pérez-González, V. H., Davalos, R. V., Lapizco-Encinas, B. H., *Electrophoresis* 2011, 32, 2456-2465.

[20] Hill, N., Lapizco-Encinas, B. H., *Anal. Bioanal. Chem.* 2020, *412*, 3891–3902.

[21] Ko, C., Li, D., Malekanfard, A., Wang. Y., Xuan, X., *Electrophoresis* 2019, *40,* 1387-1394.

[22] Bentor, J., Malekanfard, A., Raihan, M. K., Wu, S., Pan, X., Song, Y., Xuan, X., *Electrophoresis* 2021, 10.1002/elps.202100005.

[23] Roote, D. S., *In situ flushing. Technology Status Report. Ground Water Remediation Technology Analysis Center.* 1998; available at http://www.gwrtac.org.

[24] Sorbie, K. S., *Polymer-Improved Oil Recovery. Springer.* 1991

[25] Browne, C. A., Shih, A., Datta, S. S., *Nano Micro Small* 2019, 1903944

[26] Browne, C. A., Shih, A., Datta, S. S., *J. Fluid Mech.* 2020, 890 A2-1

[27] Acharya, A., Mashelkar, R. A., Ulbrecht, J., *Rheol. Acta* 1976, *15*, 454-470.

[28] Chhabra, R. P., Uhlherr, P. H. T., Boger, D. V., *J. Non-Newton. Fluid Mech.* 1980, *6*, 187-199.

[29] Zhao, C., Yang, C., *Adv. Colloid. Interf. Sci.* 2013, *201–202*, 94–108.

[30] Yeh, L. H., Hsu, J. P., *Microfluid. Nanofluid.* 2009, *7*, 383–392.

[31] Siili, D., Coutanceau, M., *J. Non-Newton. Fluid Mech.* 1977, *2*, 1-21.

[32] Li, G., Koch, D. L., *J. Fluid Mech.* 2020, *884*, A9.